Size and density sorting of dust grains in SPH simulations of protoplanetary discs

F. C. Pignatale, J.-F. Gonzalez, Nicolas Cuello, Bernard Bourdon, Caroline Fitoussi

Monthly Notices
of the
ROYAL ASTRONOMICAL SOCIETY

MNRAS **469,** 237–254 (2017)
Advance Access publication 2017 April 1

doi:10.1093/mnras/stx801

Size and density sorting of dust grains in SPH simulations of protoplanetary discs

F. C. Pignatale,[1]★ J.-F. Gonzalez,[1]★ Nicolas Cuello,[1,2,3] Bernard Bourdon[4] and Caroline Fitoussi[4]

[1] *Univ Lyon, Univ Lyon1, Ens de Lyon, CNRS, Centre de Recherche Astrophysique de Lyon UMR5574, F-69230 Saint-Genis-Laval, France*
[2] *Instituto de Astrofísica, Pontificia Universidad Católica de Chile, Santiago 8970117, Chile*
[3] *Millennium Nucleus 'Protoplanetary Disks', Santiago 8970117, Chile*
[4] *Univ Lyon, Ens de Lyon, Université Lyon 1, CNRS, UMR 5276 LGL-TPE, F-69342 Lyon, France*

Accepted 2017 March 30. Received 2017 March 30; in original form 2016 May 10

ABSTRACT

The size and density of dust grains determine their response to gas drag in protoplanetary discs. Aerodynamical (size × density) sorting is one of the proposed mechanisms to explain the grain properties and chemical fractionation of chondrites. However, the efficiency of aerodynamical sorting and the location in the disc in which it could occur are still unknown. Although the effects of grain sizes and growth in discs have been widely studied, a simultaneous analysis including dust composition is missing. In this work, we present the dynamical evolution and growth of multicomponent dust in a protoplanetary disc using a 3D, two-fluid (gas+dust) smoothed particle hydrodynamics code. We find that the dust vertical settling is characterized by two phases: a density-driven phase that leads to a vertical chemical sorting of dust and a size-driven phase that enhances the amount of lighter material in the mid-plane. We also see an efficient radial chemical sorting of the dust at large scales. We find that dust particles are aerodynamically sorted in the inner disc. The disc becomes sub-solar in its Fe/Si ratio on the surface since the early stage of evolution but sub-solar Fe/Si can be also found in the outer disc-mid-plane at late stages. Aggregates in the disc mimic the physical and chemical properties of chondrites, suggesting that aerodynamical sorting played an important role in determining their final structure.

Key words: astrochemistry – methods: numerical – meteorites, meteors, meteoroids – protoplanetary discs.

1 INTRODUCTION

In protoplanetary discs, the interaction between gas and dust plays a central role in determining the dust dynamics. The settling and drift of a dust particle due to the aerodynamic drag exerted by the surrounding gas is driven by the size and the density of the considered particle and, thus, by the stopping time,

$$t_{\rm s} = \frac{\rho_{\rm d} s_{\rm d}}{c_{\rm s} \rho_{\rm g}}, \quad (1)$$

where $s_{\rm d}$ is the size (radius) of the particle, $\rho_{\rm d}$ its intrinsic density, $c_{\rm s}$ the sound speed and $\rho_{\rm g}$ the gas density (Weidenschilling 1977). As such, for a given set of parameters ($c_{\rm s}$, $\rho_{\rm g}$), the dynamical behaviour of the particle is determined by the product of size and density, which is called the aerodynamic parameter (Cuzzi & Weidenschilling 2006), $\zeta = \rho_{\rm d} s_{\rm d}$: smaller and lighter particles have short stopping times and are well coupled to the gas while larger and denser grains have longer stopping times and are less coupled to the surrounding gas.

Furthermore, the rate of radial drift of a particle reaches its maximum when $t_{\rm s}/t_{\rm orb} = 1/2\pi$ (Weidenschilling 1977), where $t_{\rm orb}$ is the orbital period:

$$t_{\rm orb} = \frac{2\pi}{\Omega_{\rm k}}. \quad (2)$$

Thus, combining the stopping time, equation (1), with the orbital period, the optimal drift size for a given species, corresponding to the fastest drift rate, $s_{\rm opt}$, can be derived:

$$s_{\rm opt} = \frac{c_{\rm s} \rho_{\rm g}}{\Omega_{\rm k} \rho_{\rm d}}, \quad (3)$$

(Fouchet et al. 2007; Laibe et al. 2008). Equation (3) states that for given conditions, the optimal drift size varies with the intrinsic

★ E-mail: pignatale@ipgp.fr (FCP) Jean-Francois.Gonzalez@ens-lyon.fr (JFG)

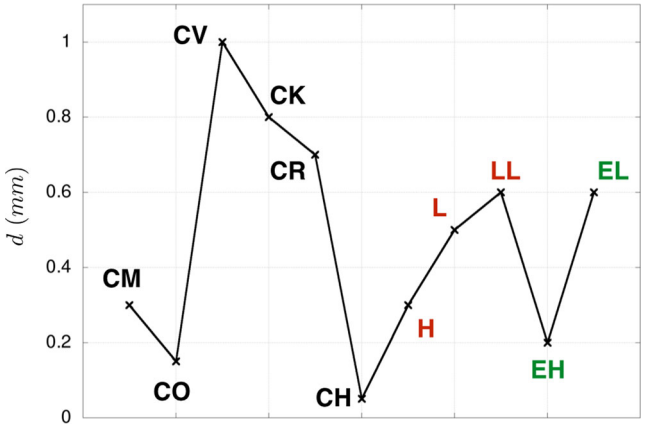

Figure 1. Average diameter of chondrules in different groups of chondrites. Figure adapted from Palme & Jones (2003) and Scott & Krot (2005).

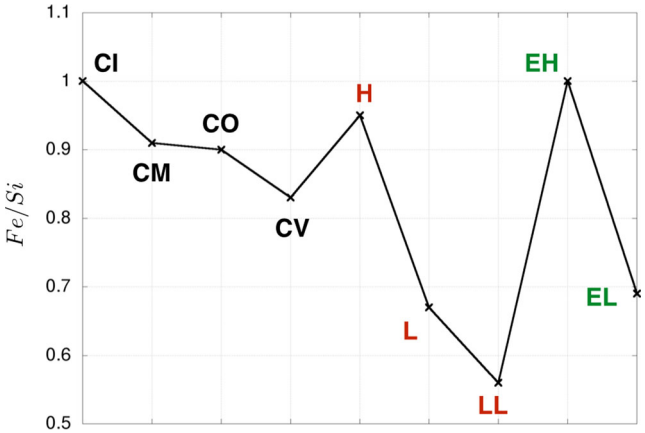

Figure 2. Fe/Si ratios for different groups of chondrites normalized to CI chondrites, which are assumed to be the solar standard. This figure is adapted from Palme & Jones (2003).

density of the considered dust particle. Moreover, the value of $s_{\rm opt}$ in the mid-plane, $s_{\rm opt}^{\rm mid}$, can be written as

$$s_{\rm opt}^{\rm mid} = \frac{\Sigma_{\rm g}}{\sqrt{2\pi}\rho_{\rm d}}, \quad (4)$$

(Fouchet, Gonzalez & Maddison 2010), where $\Sigma_{\rm g}$ is the gas surface density. The dependence of $s_{\rm opt}^{\rm mid}$ on the particle intrinsic density is also evident.

The different response to the gas drag of dusty aggregates with different sizes and densities is thought to have contributed to the determination of the physical and chemical properties of the pristine complex aggregates in our early Solar system: chondrites (Scott & Krot 2003; Cuzzi & Weidenschilling 2006). Chondrites are undifferentiated meteorites, which are characterized by the presence of chondrules, small spherules 0.01–10 mm in size (Scott & Krot 2003). Chondrites host other components: (i) calcium–aluminum rich inclusion (CAIs), made of refractory material, (ii) amoeboid olivine aggregates, characterized by fine olivine grains, metals and refractory compounds, (iii) metallic grains (Fe–Ni) and (iv) matrix, an unequilibrated volatile-rich mixture (MacPherson 2003; Scott & Krot 2003; Scott 2007). Chondrites are among the oldest rocks known. They retain radiometric ages corresponding to the first few Myr after calcium–aluminium rich inclusions [whose formation dates at 4567.2 ± 0.6 Myr ago (Amelin et al. 2002)], and thus record events that occurred at the beginning of the Solar system formation.

The formation of chondrules was an ongoing process that occurred from the formation of CAIs and lasted 3 Myr (Connelly et al. 2012). The size of chondrules varies within each clan as well as between different chondrite groups (Rubin 2010), see Fig. 1. There is a general size–density correspondence between chondrules, metallic grains (Fe–Ni) and sulphide grains, within the same group of chondrites, for which $(\rho s)_{\rm chond} \sim (\rho s)_{\rm metal} \sim (\rho s)_{\rm sulph}$ (Benoit, Akridge & Sears 1998; Kuebler et al. 1999). Size sorting and size–density sorting due to gas drag in different scenarios (local turbulences, large disc scale turbulences, jet-flow) are some of the proposed mechanisms to explain the chondrule size distribution, the assemblage of the chondrite components, and the size–density correspondence between chondrules, metallic grains (Fe–Ni) and sulphide grains, within the same group of chondrites (Clayton 1980; Benoit et al. 1998; Kuebler et al. 1999; Cuzzi et al. 2001; Liffman 2005; Zanda et al. 2006; Jacquet et al. 2012).

Chondrites exhibit different degrees of elemental fractionation, for example in their metal–silicate content (Larimer & Anders 1970). The Fe/Si ratio of chondrites normalized to CI chondrites (whose Fe/Si ratio is close to the solar value) varies according to the chondrites group (Palme & Jones 2003; Scott & Krot 2005), see Fig. 2. Moreover the ratio of oxidized iron and metallic iron+sulphides to silicon, changes for different chondrite groups, Fig. 3. The chemical and physical properties of chondrites suggest that chondrites formed, accreted and evolved in distinct disc regions and at different times, within different chemical reservoirs (Scott & Krot 2005).

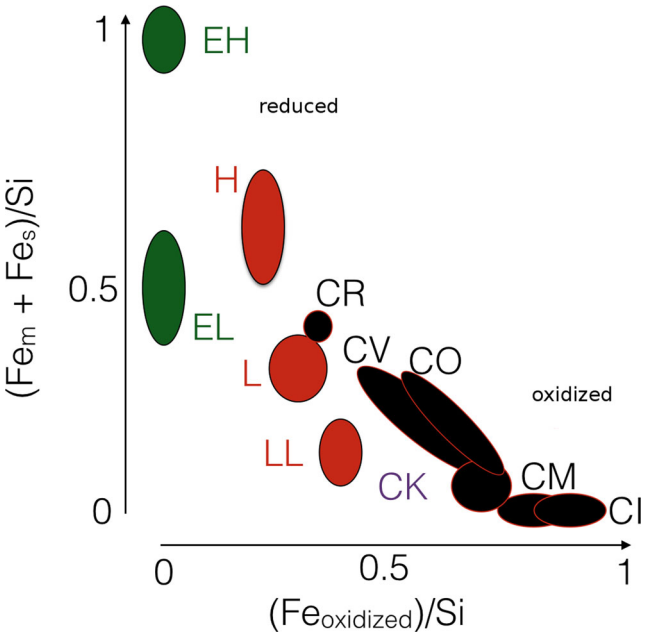

Figure 3. Urey–Craig diagram illustrating the ratio of oxidized versus metal+sulphide iron to silicon, in different groups of chondrites. Values are expressed in mole ratio. This diagram is adapted from Righter, Drake & Scott (2006).

Aerodynamic sorting, photophoresis, magnetic properties, grain aggregation and heating processes, both in large (disc, eddies) and small (chondritic parent bodies) scales, are among the suggested theories to produce the observed trend (Larimer & Wasson 1988a,b; Kuebler et al. 1999; Moore et al. 2003; Wurm, Trieloff & Rauer 2013; Cuello, Gonzalez & Pignatale 2016).

However, the level of contribution of dynamical sorting in assembling the chondritic material is not well constrained (Rubin 2010).

Size sorting of dust has been observed in protoplanetary discs. Pinte et al. (2007) modelled the dust size distribution for GG Tau, a circumbinary disc, finding that multiple populations of dust, each with different sizes and scaleheights, are necessary to match the observed brightness profile. They found that 1, 2.5, 5, 7.5, 10 μm grains have a decreasing scaleheight suggesting a stratified structure of the dust. Another T-Tauri object that shows dust sorting is TW Hya. TW Hya has been widely studied at different wavelengths, each probing different dust sizes (Wilner et al. 2000, 2003; Hughes et al. 2007, 2008; Andrews et al. 2012; Menu et al. 2014). All observations suggest that vertical and radial sorting of the dust is efficient in TW Hya: the abundance of larger grains peaks at the mid-plane and in the inner radial regions while smaller grains encompass the larger grains occupying large radial distances and vertical extension of the disc. Thus, observation suggests that sorting is a process that characterizes the dust dynamics at very large disc scales.

Several studies in the past investigated the vertical settling and radial drift of grains as a function of their size (Dullemond & Dominik 2004; Barrière-Fouchet et al. 2005; Dullemond & Dominik 2008; Ciesla 2009), and in the resulting observational properties of discs (Dullemond & Dominik 2004). An extensive review of the processes involved in gas–dust dynamics and interactions has been made by Cuzzi & Weidenschilling (2006).

In addition, the early stage of planet formation is characterized by a fast growth of submicron-size grains to large planetesimals (Dominik et al. 2007). Signatures of rapid grain growth have been extensively found in protoplanetary discs from observations at different wavelengths (Throop et al. 2001; Testi et al. 2003; Bouwman et al. 2008; Ubach et al. 2012). The growth of grains is a complex process that involves, beside the physical conditions of the disc, the chemical and physical properties of the dust (Ormel, Spaans & Tielens 2007; Blum & Wurm 2008; Okuzumi et al. 2012). Moreover, collisions of grains do not always produce perfect sticking and fragmentation and bouncing of grains upon collisions can occur (Dullemond & Dominik 2005; Zsom et al. 2010). Grain growth in protoplanetary discs has been the subject of theoretical (Stepinski & Valageas 1997; Suttner & Yorke 2001; Dullemond & Dominik 2005; Haghighipour 2005; Ciesla 2007; Laibe et al. 2008; Ormel & Klahr 2010; Birnstiel, Klahr & Ercolano 2012) and experimental investigation (Blum et al. 2000; Blum & Wurm 2000, 2008; Teiser & Wurm 2009).

However, to date, there is no complete full 3D analysis of the dust dynamics (vertical settling and radial drift) of a chemically heterogeneous dust mixture. The aim of this work is, thus, to simultaneously investigate the effects of grain growth, size and density in shaping the dust distribution of a multicomponent dust mixture at large disc scales, and to gain more insight into the dynamical processes that may have contributed to assembling chondritic material and the building blocks of planets.

2 METHODS

We compute the vertical settling, radial drift and growth of a multicomponent dust using our 3D, two-fluid (gas+dust) smoothed particle hydrodynamics (SPH) code (Barrière-Fouchet et al. 2005; Laibe et al. 2008). In this section, we describe the structure of our chosen protoplanetary disc (Section 2.1), the adopted grain chemistry (Section 2.2), the prescription used for grain growth (Section 2.3) and detail our simulations (Section 2.4).

2.1 Disc model

In order to make comparisons with previous work, we consider a typical T-Tauri disc used in Barrière-Fouchet et al. (2005) and Laibe et al. (2008) as our fiducial disc model, which represents the initial state of our simulations. The mass of the central star is $M_\star = 1\,\mathrm{M}_\odot$, and the disc is described by the following parmeters: the mass of the disc is $M_{\rm disc} = 0.02\,\mathrm{M}_\star$ with a radial extension of $20 \leq R\,(\mathrm{au}) \leq 400$. The disc is composed of 99 per cent gas and 1 per cent dust by mass. The parametrization for the temperature reads as $T \propto R^{-3/4}$, and for the surface density as $\Sigma \propto R^{-3/2}$. The disc is vertically isothermal and the sound speed is $c_{\rm s} \propto R^{-3/8}$. The vertical scaleheight is $H = c_{\rm s}/\Omega_{\rm k}$, and $H/R \propto R^{1/8}$. The disc is flared and $H/R = 0.05$ at our reference radius, $R_0 = 100$ au. For all simulations, the artificial viscosity is set to $\alpha_{\rm SPH} = 0.1$ and $\beta_{\rm SPH} = 0.0$ emulating a viscosity parameter $\alpha_{\rm ss} = 0.01$ (Shakura & Sunyaev 1973; Fouchet et al. 2007), to reproduce the observed stellar accretion rate (King, Pringle & Livio 2007).

2.2 Grain chemistry

Dust in discs is a complex mixture of several species. The chemistry of the dust is strictly related to the physical conditions in each zone of the disc and to the composition of the gas and the pristine dust (Gail 1998). In the hotter inner zone of the disc, dust experiences several chemical processes such as direct condensation from the gas phase, annealing, melting, shocks and gas-grain surface interaction (Henning & Semenov 2013). In the outer cooler part of the disc, the low temperatures and slow kinetics prevent all these processes to occur efficiently and the majority of the dust will generally keep its pristine chemical composition and structure for longer timescales. Our disc extends from $20 \leq R\,(\mathrm{au}) \leq 400$, thus we do not take in account any chemical transformation of the dust grains. Furthermore, since the inner limit of our disc is beyond the major ice lines (H_2O, CO), we do not consider any change of state (i.e. vapourization of ice particles or condensation from the gas phase). Indeed the location of the H_2O-ice line is well within our inner disc edge ($R_{\rm in} = 20$ au) when using the condensation temperatures of 145 and 170 K for H_2O-ice reported in Martin & Livio (2012). The approximate location of the CO-ice line is $16 \leq R\,(\mathrm{au}) \leq 21.5$ using the condensation temperatures of 25 and 20 K for CO reported in Mumma, Weissman & Stern (1993) and Sandford & Allamandola (1993). As such we can neglect the effect[1] of these ice-lines on the dust dynamics.

The dust mixture in our disc is taken from Pollack et al. (1994) which is representative of the dust mixture present in the outer region of protoplanetary discs. The dust is composed of water ice (H_2O), volatile organics (CH_3OH, H_2CO, $(H_2CO)_x$), refractory organics (CHON), a mixture of silicates (olivines and pyroxenes, with Fe/(Fe+Mg) = 0.3), sulphide-rich grains (namely FeS) and iron-rich grains (namely Fe), with their values of intrinsic density, $\rho_{\rm d}$, reported in Table 1 together with their weight per cent (wt%).

In Table 1, we also report some dust ratios that will be used during our discussion. They represent the ratios between the wt% of two given groups in a well-mixed disc and not the chemical ratios. In this paper, we refer to these values as 'solar' for ease of reading.

[1] The occurrence of ice lines could change the chemical composition of the dust, by removing or adding components, and alter the dust size distribution of grains. Nevertheless, the overall dynamical behaviour of grains will still be ruled by their resulting aerodynamic parameter, ζ.

Table 1. Dust distribution from Pollack et al. (1994) describing the chemical composition for large discs with related wt% and intrinsic densities. Ratios between groups of different species are also shown.

Group	Dust species	wt%	Density (g cm^{-3})
Fe	Metallic iron	1	7.87
	Troilite	6	4.83
Si	Olivine and pyroxene	25	3.46
org	Refractory organics	25	1.5
	Volatile organics	4	1
H_2O	Ice	39	0.92
		Ratios	
H_2O/Si		1.56	
Fe/Si		0.28	

In order to account for the different chemical species, we modified the SPH code described in Barrière-Fouchet et al. (2005) by introducing the possibility to assign different intrinsic density values to different particles of the dust fluid. The user can now choose a number of different dust species and the amount (wt%) of each species present in the disc. When the dust is injected in the system the SPH dust-particles are assigned with an intrinsic density according to the percentage distribution. In the present work, we follow the distribution reported in Table 1. An SPH dust particle with a given ρ_d would represent a packet of physical dust particles whose intrinsic density strongly peaks to ρ_d and where the amount of other species is irrelevant. This approach is similar to that introduced in Laibe et al. (2008) for describing the size distribution of growing particles.

2.3 Grain growth

Observations of pristine dust in protoplanetary discs are characterized by aggregates with sizes of the order of sub-microns to microns (Testi et al. 2014). In our simulations the initial grain size, s_0, is common for all particles, and is set to 10 μm. Laibe et al. (2008) show that the results of their simulations with grain growth have little dependence on s_0 when the initial size is in the sub-micron to micron range.

Aggregates in discs are made of different pristine components, which we call grains. In Section 2.2, we assumed that our initial grains comprise the species in Table 1 with their relative abundances (Pollack et al. 1994). Grain growth is a complex process, and as first order approximation one could assume that growth occurs as a result of random collision between components of the same or different species. The resulting aggregates would be characterized by a distribution of densities which ranges between the two extremes we consider here (iron and ice), with populations of iron-, silicate- and ice-enriched grains. Due to the initial abundance differences of our species, the resulting aggregates will maintain a spread in their densities, as it is unlikely to produce only one single final group of aggregates characterized by the same type of mixture.

Dynamics dictates how aggregates will evolve in a disc. Laibe et al. (2008) and Laibe (2014), Laibe, Gonzalez & Maddison (2014a), Laibe et al. (2014b) investigated in detail the differences in the time-scales between vertical settling and growth rates, and between radial drift and growth rates. They concluded that the vertical settling is almost one hundred times faster than the radial drift, and that these two dynamical events can be considered as separate. Moreover, grains grow moderately during the settling phase compared to their final size ($s = 100$ μm, at 100 au, see Appendix A) and the efficiency of growth increases once the grains settle in the mid-plane.

Since the initial size of our grains, s_0, is equal and common for all particles (10 μm), grains with different compositions will behave differently as their stopping time is a function of their density (see equation 1). Given the moderate growth of grains during vertical settling, the settling can result in inhomogeneities in the chemical content of the disc. In the mid-plane, the radial drift is then dictated by ζ (Weidenschilling 1977). Aggregates of the same size but different compositions will drift at different velocities. These considerations suggest that grain dynamics in the disc should, in fact, enhance chemical inhomogeneity. Pieces of evidence from meteorites also point to the presence in the Solar Nebula of different chemical reservoirs from which they accreted (Palme & Jones 2003; Scott & Krot 2005). The verification of these predictions and their evolution with time are some of the goals of this work.

Grain growth in our SPH code follows Laibe et al. (2008). Grains within an SPH dust particle are assumed to stick perfectly upon collision. Our prescription for grain growth is taken from Stepinski & Valageas (1997), where $\mathrm{d}s/\mathrm{d}t$ is described by the following equation:

$$\frac{\mathrm{d}s}{\mathrm{d}t} = \sqrt{2^{2/3} R_0 \alpha}\, \frac{\hat{\rho}}{\rho_d} c_s \frac{\sqrt{\mathrm{Sc} - 1}}{\mathrm{Sc}}, \tag{5}$$

where R_0 is the Rossby number, α the Shakura & Sunyaev (1973) turbulence parameter, $\hat{\rho}$ the density of matter concentrated into solid particles, ρ_d the intrinsic density of the physical grains and Sc the Schmidt number.

In our simulations when aggregates grow they keep their intrinsic density constant, i.e. there is no mixed growth between particles of different species. This as a direct consequence of the growth prescription of Stepinski & Valageas (1997) which assumes collisions occur each time between two identical (size and density) spherical particles with growth occurring within an SPH particle (Laibe et al. 2008).

While it may appear non-physical to only consider growth between the same species, this simplified assumption does mimic the true density distribution of real growth between species of mixed composition. The initial difference in the abundances of components–grains and their dynamical dependence on density suggest that we will have, at any given time and location, aggregates with different compositions. Aggregates whose resulting density is iron-enriched will behave similarly to our 'iron grains', while aggregates that are characterized by a high ice content will behave similarly to our 'ice grains', and silicate-rich grains will behave similarly to our 'pure silicates'. As such, having a fixed discrete distribution of ρ_d between two extremes (ice and iron) and four intermediate species will allow us to trace and investigate the different behaviours driven by the intrinsic density and the aerodynamic parameter. Any interpolation of the behaviour of aggregates with intermediate densities is then straightforward. In fact, this approach is similar to the widely used approximation to study the effect of size on dust dynamics for which a discrete grain size distribution and often one chemical species is considered (Barrière-Fouchet et al. 2005; Dullemond & Dominik 2008; Bai & Stone 2010; Charnoz & Taillifet 2012). These simulations proved to be in very good agreement with observations. Our simulations, instead, account for a discrete distribution of densities and a time-evolving distribution of size since we also include grain growth. Growth can erase the illustrated effect of densities only if, at any given time and location,

grains with different composition reach the same value of ζ before any of the dynamical forces (drift and settling) separate them. We demonstrate in Appendix A, that this is never the case.

In our simulations, we do not consider dust fragmentation. Fragmentation occurs when the relative velocity of the particles becomes greater than the critical velocity (the velocity between colliding particles which will likely lead to a fragmentation of the dust rather than sticking) (Blum & Wurm 2008). The dynamics of growing and fragmenting dust of single composition have been studied in detail by Dullemond & Dominik (2005), Birnstiel, Dullemond & Brauer (2010), Birnstiel et al. (2012), Gonzalez et al. (2015a) and more recently by Gonzalez, Laibe & Maddison (2017). Dullemond & Dominik (2005) and Birnstiel et al. (2010, 2012) showed that a balance between growth and fragmentation can result in a steady distribution of different sizes in discs, especially in the inner disc zones. Gonzalez et al. (2017) found that growing and fragmenting grains can result in a self-induced dust trap.

The critical velocity is a function of the chemical composition and the porosity of the dust (Yamamoto, Kadono & Wada 2014). Preliminary tests for our disc model with the most recent theoretical values of 30–36 m s^{-1} derived from Yamamoto et al. (2014) for silicate aggregates made of monomers of 0.1 μm, show that this critical velocity is hardly reached in our large disc, and the effects of fragmentation are negligible within the considered evolutionary time. We assume that no changes in the critical velocities occur with time, size of grains (always considered as grains made of monomers of 0.1 μm) and species. However, critical velocities of different species, such as ice, silicates, iron and sulphides, are still uncertain (Teiser & Wurm 2009; Wada et al. 2009, 2013; Yamamoto et al. 2014) and they need to be assessed before implementation.

For this reason, we decided not to include fragmentation at this stage. Fragmentation of grains will be investigated in a future work.

2.4 Simulations

In order to understand the effect of multiple intrinsic densities in shaping the chemical content of our disc, we run a simulation with the dust distribution listed in Table 1 with grain growth. As mentioned in the previous section, the initial grain size, s_0, common for all particles, is set to 10 μm.

Similarly to Barrière-Fouchet et al. (2005) and Laibe et al. (2008), the simulation starts at $t = 0$ with a gas disc that is relaxed[2] for $t \sim 8000$ yr. At that time, the dust particles are injected in the system on top of the gas particles [see Barrière-Fouchet et al. (2005) for details]. The system then evolves for a total of $t \sim 1.6 \times 10^5$ yr, after which the disc reaches a steady state: the majority of the dust particles decouples from the gas and settles in the mid-plane, while the grain-growth becomes less efficient. This simulation is run in high resolution with a total of 400 000 SPH particles.

3 RESULTS

In this section, we present the resulting evolution of dust particles in our disc. First, we focus on the growth profile (3.1) and then on the vertical settling (3.2) and radial drift (3.3) of the dust particles.

[2] Same as in Barrière-Fouchet et al. (2005) and Laibe et al. (2008) the gaseous disc is evolved for a given time to let the pressure and artificial viscosity smooth the initial velocity field and the shape of the gaseous disc. Moreover, particles which, at any given time, move out the disc boundaries are removed from the calculation.

3.1 Grain growth

Fig. 4 shows the evolution of grain growth as a function of the distance from the star at four different evolutionary stages. The orange line with open squares and the brown line with open triangles represent respectively the $s_{\rm opt}^{\rm mid}$ for water ice and iron calculated following equation (4). Being function of the intrinsic density, the $s_{\rm opt}^{\rm mid}$ lines for silicates and sulphides, not shown in the figure, will lie in between.

It can be seen that growth proceeds very rapidly in the inner disc with particles reaching cm-sizes in a few thousand years. Similarly to Laibe et al. (2008), our simulation shows that efficient growth is experienced by grains in the inner region and, as expected, we see that denser grains generally reach smaller sizes. This behaviour results directly from the prescription of growth derived by Stepinski & Valageas (1997), with $\mathrm{d}s/\mathrm{d}t \propto c_{\rm s}\rho_{\rm d}^{-1}$.

One may wonder why grains having reached their optimal drift size are not lost to the star but stay in the inner disc where they continue to grow, and whether this is a numerical artefact. In their SPH simulations, Lodato & Rice (2004) found that the inner boundary conditions produced an outward erosion of the disc inner edge resulting in a gas pressure maximum slightly exterior to it, which would be capable of trapping drifting grains. However, the expectation that fast-drifting grains leave the disc before reaching large sizes comes from analytical (Weidenschilling 1977) and numerical (Brauer, Dullemond & Henning 2008a; Birnstiel et al. 2010) work neglecting the drag back-reaction of dust on gas. On the contrary, several studies taking back-reaction into account (see e.g. Laibe et al. 2008; Fouchet et al. 2010; Gonzalez et al. 2015a; Drążkowska, Alibert & Moore 2016) have shown that it slows down the drift of grains and, combined with their faster growth closer to the star, results in a pile up in the inner disc. This is also what happens in the simulation presented in this paper (for a detailed discussion of the role of back-reaction, see Gonzalez et al. 2017).

In Laibe et al. (2008) the evolution of the radial size profile is driven by the rate of radial drift caused by the optimal drift size of one species, ice. In our case, the evolution of the growth profile is not only driven by the size of the particles, but by the aerodynamic parameters ($\zeta = \rho s$), and by the optimal drift size proper to each species (see equations 3 and 4). The effects of grain growth on the evolution of the dust distribution will be discussed in detail in Sections 3.3 and 4.

3.2 Vertical settling

Fig. 5 shows the distribution of the icy (water ice plus organics), silicates, sulphides and iron particles respectively, at four evolutionary stages for the disc seen edge-on: a fast vertical settling is followed by a very efficient radial drift of denser particles. It is evident that the chemical characterization of the dust particles is driving the dynamics of the dust at different rates.

In Fig. 6 (top) we report the altitude Z as a function of time for three particles with different intrinsic density (water ice, silicate and iron) which are located at the same position ($R \sim 100$ au, $Z \sim 9$ au) at the beginning of the simulation. In Fig. 6 (middle) we report the ratio $s_{\rm ice}/s_{\rm sil}$ (red) and $s_{\rm ice}/s_{\rm iron}$ (blue) as a function of time, while Fig. 6 (bottom) shows the grain size as a function of time for the three considered species. In Fig. 7, we show the evolution of the aerodynamic parameter for icy particles (black) and silicate particles (red) at the same evolutionary stages as in Fig. 5. Fig. 7 allows to analyse the global evolution of the aerodynamic parameter of all the selected particles.

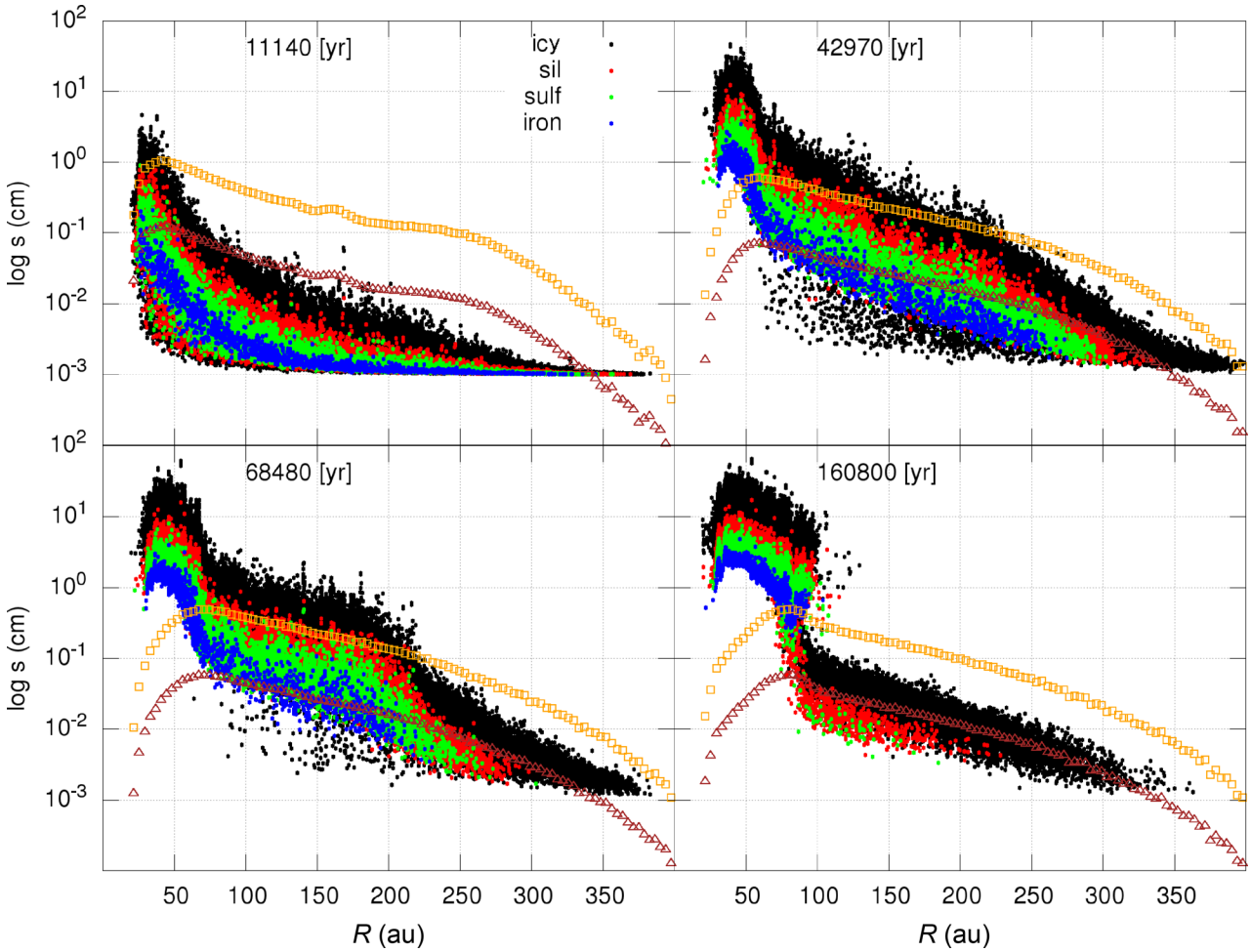

Figure 4. Radial size distribution for icy (black), which comprise water ice, volatile organics and refractory organics, silicates (red), sulphides (green) and iron (blue) particles at four evolutionary stages. Species are superimposed for ease of reading. The two curves represent the optimal drift size for water ice (orange with open squares) and iron (brown with open triangles), calculated using equation (4). Grain growth proceeds faster in the inner zones than in the outer zones. Moreover, the optimal drift size is a function of the intrinsic density of the dust. Thus, denser grains will have a smaller optimal drift size compared to lighter grains. Since grains are growing, denser particles will start their radial drift at earlier stages in the outer disc, leading to a radial chemical sorting.

At early stages of our simulation, the dust motion is dominated by vertical settling which lasts $t \sim 40$–50 kyr. Looking at Fig. 5, we can distinguish two phases of vertical settling. First, the disc experiences a vertical chemical sorting with heavier particles populating a thin section of the disc. The disc assumes a chemically layered structure with icy particles occupying a larger vertical section. Moving from the surface of the disc towards the mid-plane, the icy disc becomes enriched in silicates, and then in sulphides. In the mid-plane, the dust will be iron enriched. This efficient vertical separation occurs over very short time-scales. In the case reported in Fig. 6, particles reach their maximum vertical separation within a few hundred years. As the dust is injected at $t \sim 8$ kyr, within $t \sim 3$ kyr the disc is chemically vertically sorted in its large scale (see Fig. 5).

This first phase of settling can be better explained by looking at the time-scale of vertical settling for a dust grain in a disc, keeping in mind that at the beginning of the simulation grains have the same size (ζ_i differs only because of their intrinsic density). From Dullemond & Dominik (2004),

$$t_{\rm sett} = \frac{Z}{v_{\rm sett}} = \frac{4}{3}\frac{\sigma}{m}\frac{\rho_{\rm g} c_{\rm s}}{\Omega_{\rm k}^2}, \qquad (6)$$

where m is the mass of a spherical particle and σ its cross-section. Given that $(\sigma/m) \propto (\rho_{\rm d} s)^{-1} = \zeta^{-1}$, equation (6) states that, for given conditions, $(\rho_{\rm g} c_{\rm s}/\Omega_{\rm k}^2)$, and distance to cover, Z, larger-heavier particles will have smaller $t_{\rm sett}$ or will settle at higher speed than smaller-lighter particles. In this case, two grains made of different material, i and j, but with the same size would have $(t^i_{\rm sett}/t^j_{\rm sett}) \propto (\rho_j/\rho_i)$. As an example the $t^{\rm ice}_{\rm sett}$ is $8.55 = (7.87/0.92)$ times longer than $t^{\rm iron}_{\rm sett}$, and in order to erase the effect of density ice particles should grow 8.55 times larger than the iron particles before they separate. Fig. 6 (middle and bottom) shows that during the first phase of vertical settling growth is not efficient to counterbalance the strong effect brought by the intrinsic density of grains (in the first couple of kyr of our simulation the $s_{\rm ice}/s_{\rm iron}$ ratio is always of the order of 1–1.2. Thus, when the size of two particles is comparable, which is the case in the early evolution, the vertical settling is density driven.

A second phase of vertical settling starts immediately in the inner disc and, at later times, in the outer disc: the icy particles settle towards the mid-plane, remixing with the silicate–iron-rich dust. This second stage of vertical settling can be explained by the evolution of the aerodynamic parameter for single species. In

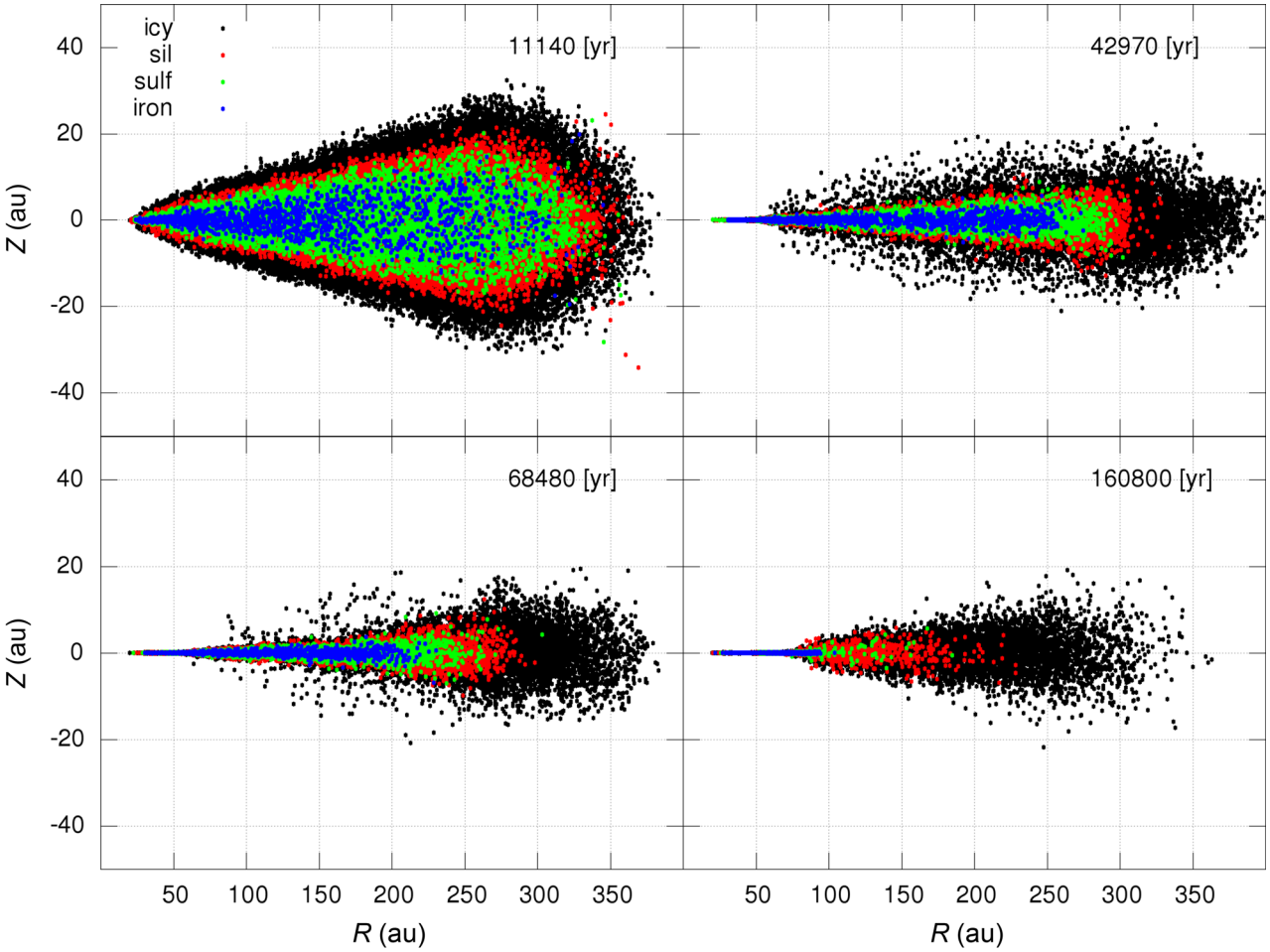

Figure 5. Edge-on view of the spatial evolution for icy (black), silicate (red), sulphide (green) and iron (blue) grains at four evolutionary stages. Species are superimposed for ease of reading. A fast dust vertical settling is followed by an efficient dust radial drift. The effects of different dust chemistry in determining the rate of settling and drift are evident.

Fig. 7 the icy particles for which $\zeta_{\rm icy} < \zeta_{\rm sil}$, are the particles that populate the icy contour of the disc in Fig. 5. As grain growth proceeds, ζ of the lighter material on the surface of the disk increases and becomes comparable to the values that characterized the denser material at earlier stages. We have a superimposition of the ζ values with $\zeta_{\rm icy} \sim \zeta_{\rm sil}$ and the vertical settling of the lighter material becomes more efficient. This phase of settling is, thus, size driven.

The introduction of lighter material into the mid-plane is more efficient in the inner zone of the disc (see Fig. 5). At the end of our simulation and in the inner ∼80 au, all the icy particles are introduced in the denser mid-plane. In the outer part of the disc a vertical chemical sorting can still be noticed. This behaviour is due to the lower growth rate in the outer disc [see Fig. 4, and Laibe et al. (2008)], where smaller and lighter icy grains will remain coupled to the gas longer.

3.3 Radial drift

After the first ∼40–50 kyr, the radial drift of the dust starts to become extremely efficient for the denser grains (see Fig. 5). We see a radial sorting of chemical species with time. The outer disc becomes depleted in heavy particles in $t \sim 50$ kyr. Fig. 8 shows the surface density of different species at the end of the simulation: the disc outside ∼110 au is iron depleted, outside ∼200 au sulphide depleted and outside 250 au silicate depleted. The regions beyond 250 au are ice rich. The different maximum values of the surface densities are due to the differences in the initial amount that characterizes each species.

As reported in the introduction, the dust radial drift is driven by the optimal drift size proper to each dust particle (see equations 3 and 4). In Fig. 4, we reported the evolution of the radial profile of $s_{\rm opt}^{\rm mid}$ for water ice and iron at different evolutionary stages. Iron particles have a smaller optimal drift size than water ice particles. Looking at Fig. 4 it can be seen that the smaller optimal drift size for iron particle is leading to a radial chemical sorting of the dust. Similar to iron, sulphides and silicates follow the radial drift dictated by their $s_{\rm opt}^{\rm mid}$. Not all the water-ice particles in the outer disc reach their optimal drift size by the end of the simulation, making the radial drift of ice overall less efficient.

Fig. 9 tracks the radial drift (top), $s/s_{\rm opt}$ (middle), with $s_{\rm opt}$ calculated using equation (3), and the size (bottom) as a function of time for three particles with different intrinsic density (water-ice, silicate and iron) which are located at the same position at the beginning of the simulation. As the growth proceeds, the iron particle reaches the $s/s_{\rm opt} = 1$ point before the lighter particles and starts to drift inward more efficiently. Lighter particles keep growing in place before reaching their optimal size and starting to drift towards the inner regions of the disc.

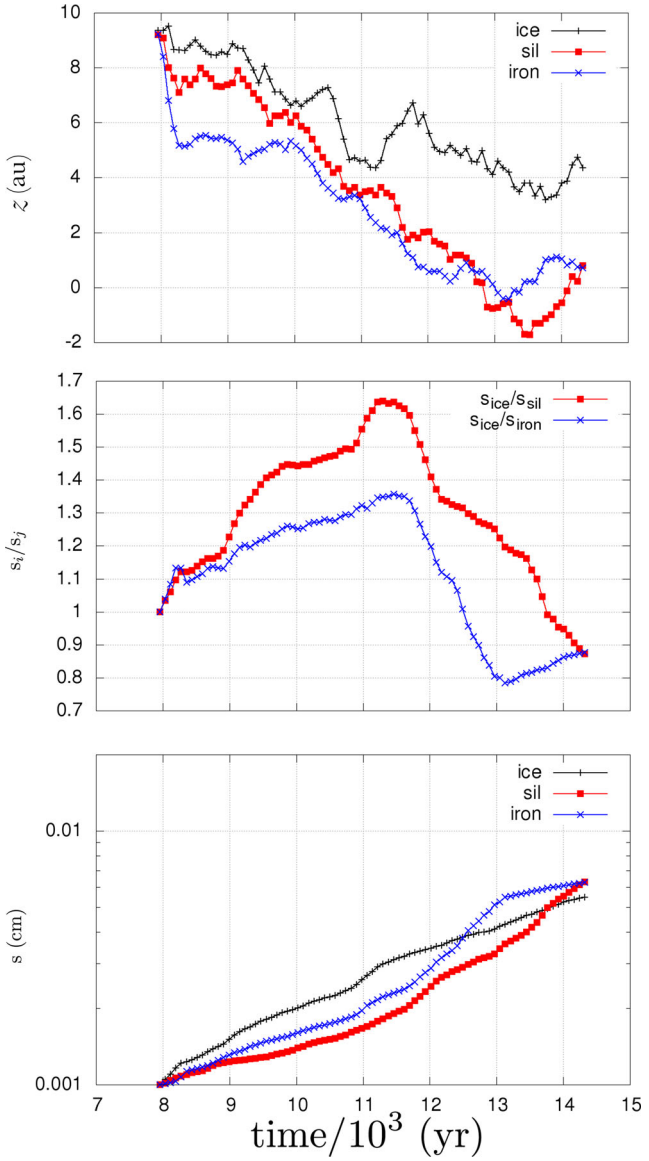

Figure 6. Top: time evolution of the altitude of water ice (black), silicate (red), iron (blue) particles that lie at the same position ($R \sim 100$ au, $Z \sim 9$ au) at the beginning of the simulation. Middle: time evolution of $s_{\rm ice}/s_{\rm sil}$ (red) and $s_{\rm ice}/s_{\rm iron}$ (blue) ratio. Bottom: size as a function of time for the three different particles. At the beginning of the simulation when the size of the particles is comparable, the vertical settling is density driven and will lead to a vertical chemical separation according to the intrinsic density of the grains. The curve of the s_i/s_j ratios reaches a peak after 11 kyr and then decreases: ice particles grow bigger, thus the ratio increases. When the silicates and iron particles settle towards the mid-plane, they grow faster than ice, as they are in a denser environment, and thus the s_i/s_j ratios starts to decrease. However, after a few thousand years we are already tracing particles that are far from each other and, thus, experiencing different local conditions.

4 DISCUSSION

Our results are in good agreement with those found by Laibe et al. (2008), Laibe (2014), Laibe et al. (2014a) and Laibe et al. (2014b), who studied the dynamics of growing but not fragmenting grains illustrated in Section 2.3. Furthermore, we confirm that, (i) a very efficient vertical chemical sorting of the dust starts at the beginning of the simulation, and (ii) the density-driven vertical settling that produces the initial chemical sorting is the first dynamical mechanism expected when the size of the grains is comparable. Moreover, the grain growth within our disc model is not efficient enough to counterbalance this process.

Our results show that, as the intrinsic density of the growing grains determines the optimal drift size, the radial drift of different species would produce a radial chemical sorting of the dust. As a consequence of the vertical settling and radial drift, the disc will lose its initial chemical homogeneity, with inhomogeneities occurring from the beginning of the simulation. These results could bring dramatic consequences in the composition of the building block of meteorites parent bodies and planetesimals. The chemical and dynamical evolution of the dust in our disc is thus the main focus of this section. We will discuss the physical properties of the particles in Section 4.1 and the evolution of the chemical content in our disc in Section 4.2.

4.1 Size and density sorting

Using our set of diagnostic we are able to trace all the properties of every SPH particle at any given time. At the end of the simulation, we randomly sampled groups of water ice and silicates particles that are located at the same coordinates in the mid-plane and record their size and intrinsic density. We replicate this measurement at different radial distances from the central star. We chose ice and silicates particles as they are still present at large radial distance at the end of the simulation. In Fig. 10, we thus plot the average size of water-ice particles versus the average size of silicate particles at different radial distances from the star (colours). The brown line represents the theoretical size of water-ice particles predicted by the following equation:

$$s_{\rm ice} = s_{\rm sil}\frac{\rho_{\rm sil}}{\rho_{\rm ice}}, \tag{7}$$

i.e. the predicted size of water-ice particles if perfect size–density sorting with silicates particles occurs [$\zeta_{\rm ice} = \zeta_{\rm sil} = (s\rho)_{\rm ice} = (s\rho)_{\rm sil}$].

The returned correlation coefficient between the average size of silicates and average size of the ice particles for all the data points within $R < 100$ au in Fig. 10 is $R_{\rm c} = 0.99$, while for the points laying at $R \geq 100$ au the correlation coefficient is $R_{\rm c} = 0.64$. The inner mid-plane of the disc is generally aerodynamically (size–density) sorted. This is less evident in the outer part of the disc, where the lower growth rate and the lower gas density cause the aerodynamic sorting to occur more slowly. Thus, in case of pure growth particles tend to naturally sort in the disc according to their aerodynamic parameter.

Our finding confirms that aerodynamic sorting can be an active mechanism that characterizes the disc at very large scales and suggest that the sorting trend observed in chondrites could thus have occurred not only in a local environment but also at disc scales. Since the aerodynamic sorting in chondrites could have occurred between chondrules and metal-troilite grains within the same chondrite group (Benoit et al. 1998; Friedrich et al. 2015), we investigate the aerodynamic sorting between different species in more detail in Section 4.2.1.

4.2 Disc chemical and dynamical evolution

As discussed in Section 3, vertical settling and radial migration continuously change the distribution of dust particles in different regions of the disc.

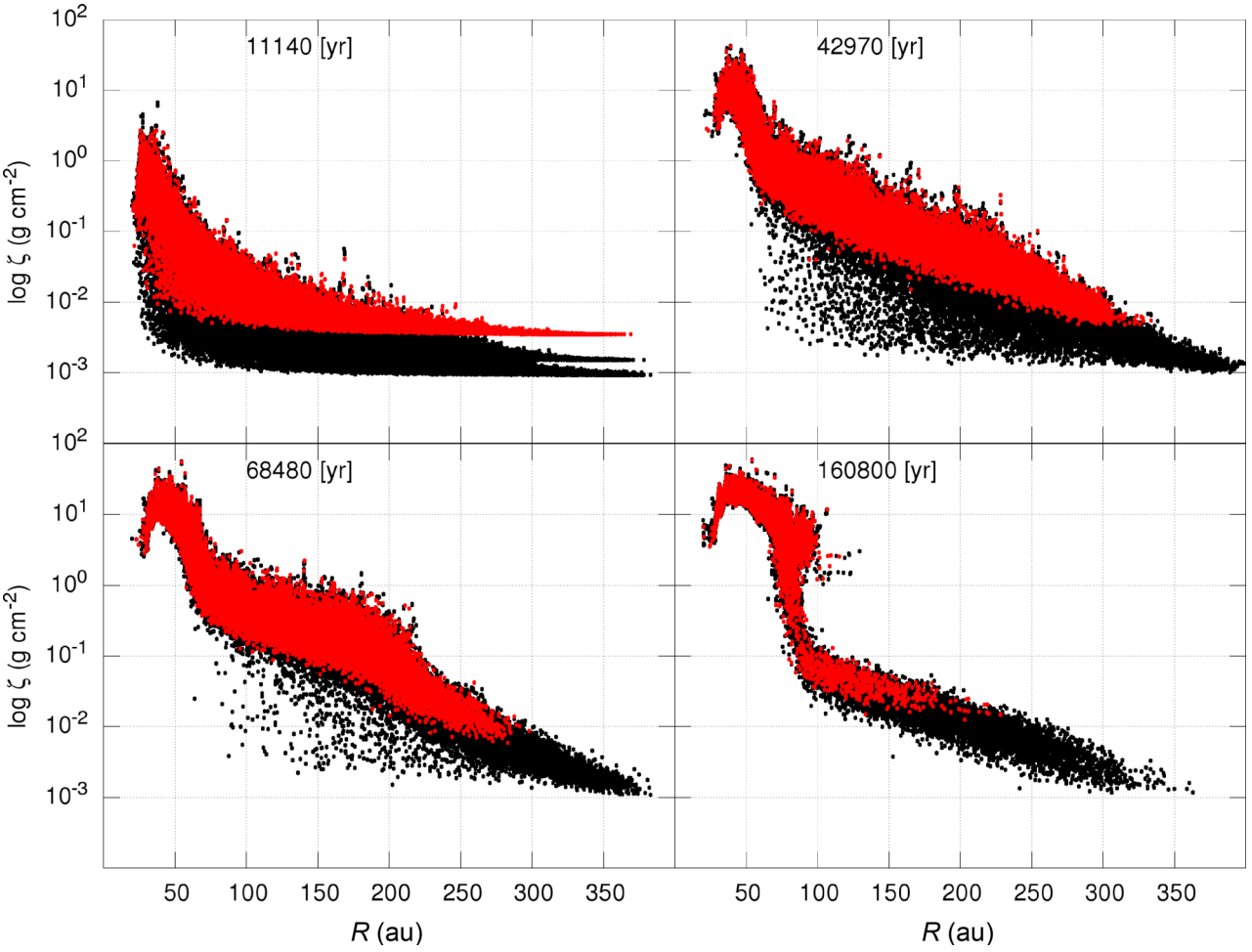

Figure 7. Aerodynamic parameter for icy (black) grains and silicates (red) grains at four evolutionary stages. The double tail for the icy grains is caused by the fact that we are considering all the three icy populations (water ice, volatile organics and refractory organic) that have intrinsic density $0.92 \leq \rho_{\rm d} \leq 1.5$. When the size of the grains with different density is comparable, the heavier grains separate from the lighter grains and start to settle towards the mid-plane. As the lighter grains grow, their aerodynamic parameter increases and they start to behave as heavier grains and settle towards the mid-plane. After $t \sim 50$ kyr, the vertical chemical separation of grains in the inner disc out to 80 au is lost.

In order to quantify in more details the change in the chemistry in the whole time range, we report in Fig. 11, from left to right, the evolution of the dust mass content (normalized to the mass present at the beginning of the simulation), the evolution of the H_2O/Si and Fe/Si ratios[3] (all values normalized to our 'solar' values in Table 1), in the disc mid-plane ($-1 < Z\,({\rm au}) < 1$) (top row), and in the disc surface where $|Z\,({\rm au})| > 1$ (bottom row). The selected disc radial extension is $20 < R\,({\rm au}) < 100$.

The H_2O/Si and Fe/Si ratios at the surface of the disc are plotted until the dust mass, $m_{\rm d}$, drops to 10 per cent of the initial mass. Close to this value, the ratios are biased by the small number of particles present. The time resolution of all the plots is $\Delta t \sim 159$ yr. This allows to investigate the variation with time of the chemical content in our disc in very good detail, as this value represents 1/1000 of the total time of the simulation. Moreover, these plots will give us an idea of the chemical composition of the dust from which aggregates could accrete at a given time.

Looking at Fig. 11, the effects of the dynamics on the chemical distribution of the dust become clearer. For the H_2O/Si ratio, in the mid-plane, we see (1) the enhancement of silicate particles due to the density-driven vertical settling; (2) the size-driven vertical settling then increases the amount of ice which is populating the mid-plane. When the dust radial drift starts to become more efficient, (3) we see that silicate particles from the outer disc are populating the inner disc mid-plane, thus decreasing the H_2O/Si ratio. At later stages, (4) the radial drift of the ice increases the H_2O/Si ratio. On the other hand, for the Fe/Si ratio, we see (1) the enhancement of iron due to the density-driven vertical settling; (2) the amount of silicate particles is then increased by the size-driven vertical settling. When the dust radial drift starts to become more efficient (3) iron particles populate the inner disc mid-plane, and, at later stages, (4) the radial drift of the silicates decreases the Fe/Si ratio.

At the same time, on the surface of the disc, the dust content is reduced in heavier compounds. The H_2O/Si ratio increases due to the vertical settling of the silicate particles. The trend does not change with time as the vertical settling of the icy particles

[3] As pointed out in Section 1, these ratios are the ratios between the number of particles belonging to two of the different groups (Fe, Si, H_2O) that are populating a given region at a given time. For example, the Fe/Si ratios is

$$\mathrm{Fe/Si} = (n_{\rm iron}/n_{\rm sil}). \quad (8)$$

All values are then normalized to the 'solar' values in Table 1.

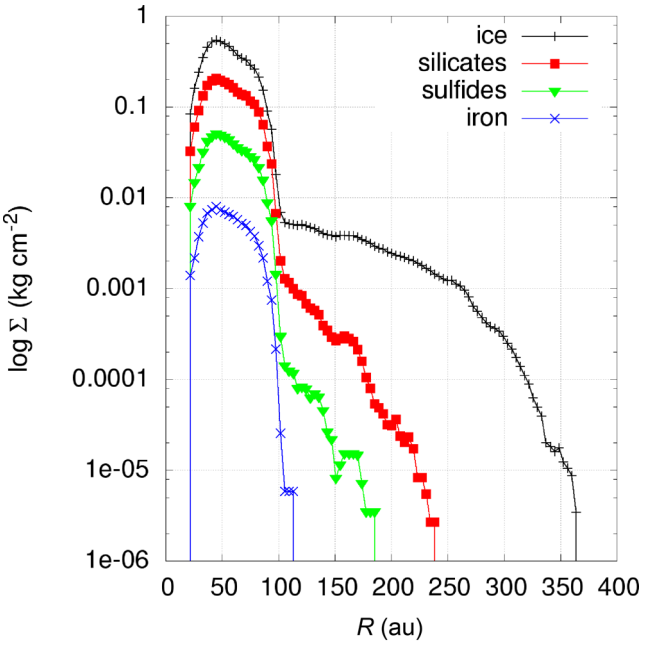

Figure 8. Surface density of water-ice, silicates, sulphides and iron particles at the end of the simulation. The chemical radial sorting is evident. The differences in the values of the surface densities are due to the different initial amount which characterizes each species.

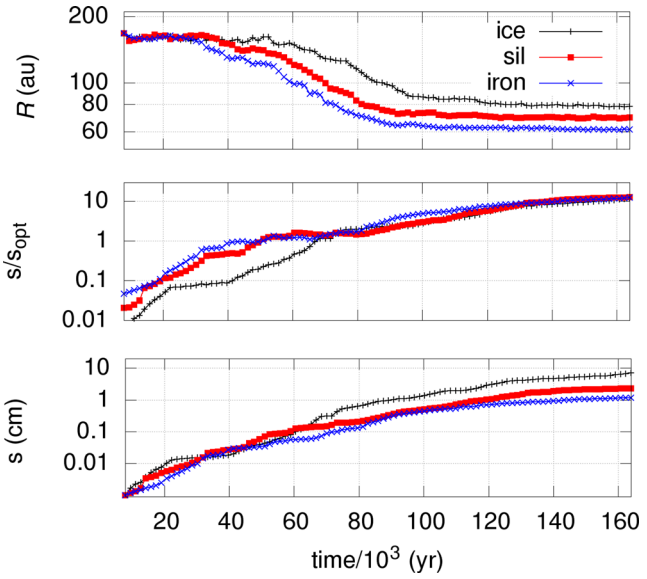

Figure 9. Top: radial drift for water ice, silicates and iron particles as a function of time. $s/s_{\rm opt}$ (middle) and s (bottom) as a function of time for the same particles. Denser particles have smaller optimal drift size. As particles grow, iron particles reach their optimal drift size before lighter particles and thus, start to drift inward before the lighter particles.

does not become so efficient to invert and lower the H_2O/Si ratio within the time ($t \sim 20$ kyr) for which we reach the cut-off (the mass of the particles present in the selected zone reaches 10 per cent of the initial mass). The Fe/Si ratio becomes 'sub-solar' due to the vertical settling of the iron particles, until the density-driven phase is replaced by the size-driven phase when silicate particles also start to settle more efficiently due to their growth. As a consequence the Fe/Si ratio starts to move again towards higher values.

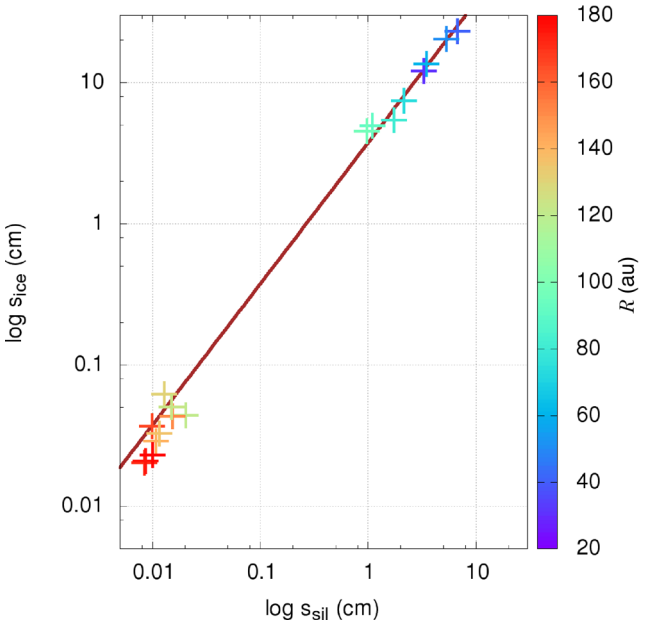

Figure 10. Average size of silicates versus average size of ice particles at different distances from the protostar (colour). The brown line represents the theoretical size of ice grains predicted using equation (7). The dust in the inner disc ($R < 100$ au) is aerodynamically sorted with a correlation coefficient of 0.99. This sorting is less evident beyond 100 au, where the predicted trend is not fully satisfied with a correlation coefficient of 0.64.

Similarly to Fig. 11, in Fig. 12 we report the dust mass ratio and the chemical ratios in the disc mid-plane (top) and surface (bottom) for $100 < R\,(\rm au) < 200$. We see a different behaviour of the mass of particles that populate the disc mid-plane at different times: (a) the amount of dust in the mid-plane increases due to the dust vertical settling, and (b) at $t \sim 50$ kyr due to the radial drift of the dust coming from the outer regions of the disc. The behaviour of the chemical ratios at these early stages is similar to that found in Fig. 11. However, at $t \sim 80$ kyr we see (c), a steep decrease of the dust mass of the disc and, at the same time, a decrease of the Fe/Si ratio. At $t \sim 120$ kyr, (d), a second fast depletion of dust occurs and the H_2O/Si increases. This behaviour can be explained by the radial drift of the iron particles which starts as soon as their optimal drift size is reached (c), and then by the radial drift of silicates particles, when they reach their $s_{\rm opt}$ at later stage (d) (see also Fig. 9).

On the disc surface the chemical ratios are characterized by the similar behaviour found in Fig. 11 for the early evolutionary stage: in this part of the disc surface, the Fe/Si ratio drops to 'sub-solar' values (density-driven settling) before returning to 'supersolar' values (size-driven settling). The H_2O/Si ratio increases because of the density-driven vertical settling of the silicates, then decreases because of the size-driven vertical settling of the ice particles.

The second drop in the Fe/Si ratio which starts at $t \sim 60$–80 kyr, is then due to the radial drift of the iron which at this stage is more efficient than the silicates one, and the H_2O/Si ratio increases because of the radial drift of the silicates which is more efficient than the ice one. However, at this stage, the total mass in this region already dropped under 20 per cent of the initial value and the results start to get biased by the small number of particles.

In conclusion, when we look in this disc zone, we are also observing the transit of the denser dust that is leaving the outer regions of the disc and crossing this zone to populate the inner disc.

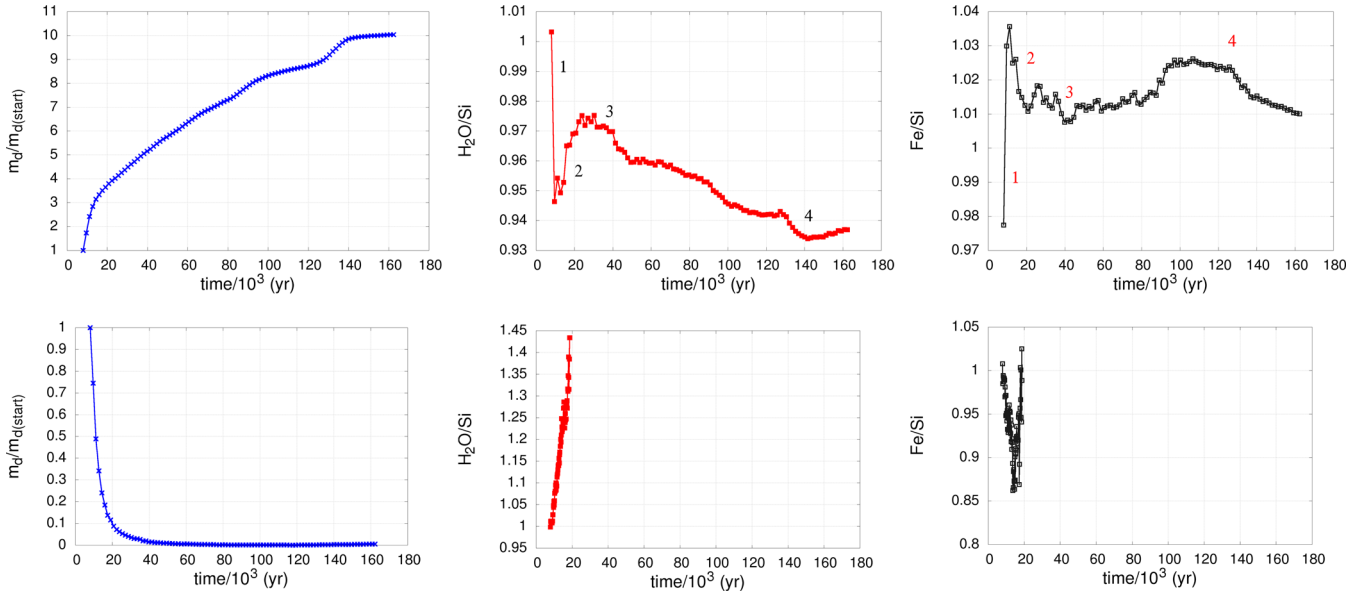

Figure 11. Top row: time evolution of the dust mass content compared to the initial mass present in the mid-plane, $-1 < Z\,(\mathrm{au}) < 1$, where $20 < R\,(\mathrm{au}) < 100$ (left), H_2O/Si (centre) and Fe/Si (right) ratios in the considered zone. The changes in the chemical ratios brought by the dust dynamics are evident: (1) the density-driven vertical settling, (2) the size-driven vertical settling, (3) the efficient radial drift of denser dust, (4) the radial drift of the residual lighter dust. Bottom row: same as top row for the disc surface where $|Z\,(\mathrm{au})| > 1$. The chemical ratios of the disc surface are plotted until $m_\mathrm{d}/m_{\mathrm{d(start)}}$ reaches 10 per cent of the initial mass.

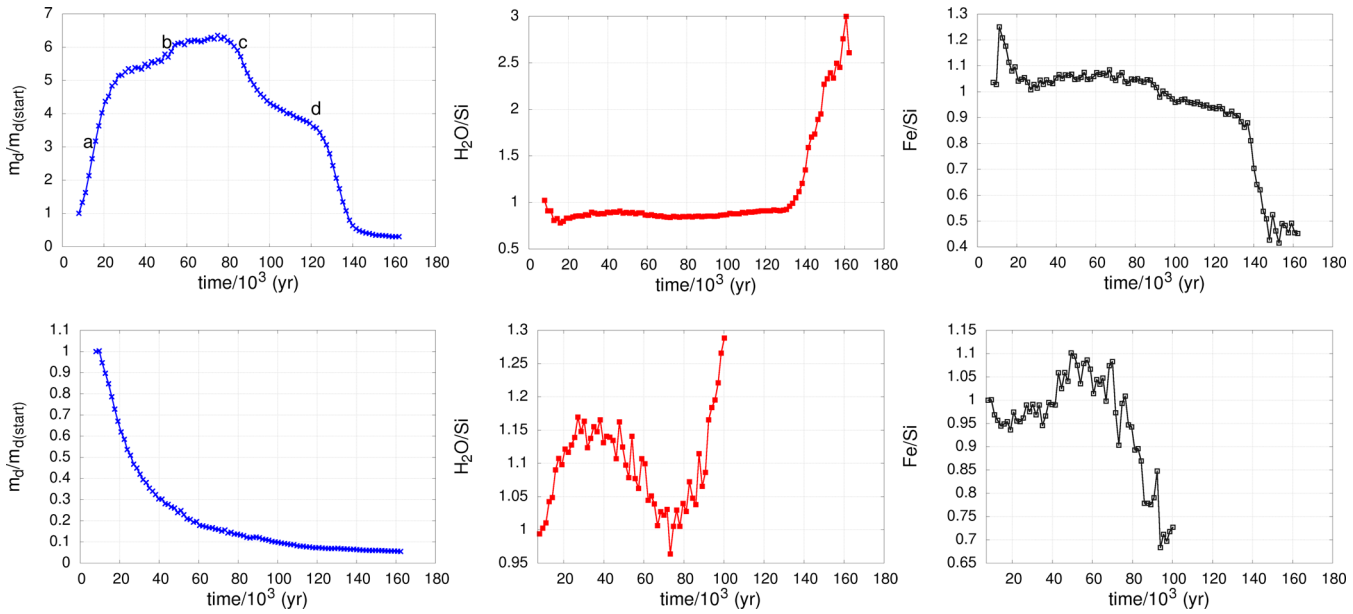

Figure 12. Same as Fig. 11 with $100 < R\,(\mathrm{au}) < 200$, in the mid-plane, top row and surface, bottom row. Letters in the dust mass plot describe the different phases of vertical settling and radial drift (see text).

4.2.1 Analogies with chondrites

In the previous sections, we showed that at early stages, when the size of the pristine dust is comparable, the density-driven vertical settling will separate the denser particles from the lighter particles leading to dust chemical sorting. Our results also show that chemical sorting can also occur via radial drift: the resulting inner disc is enriched with denser material while the outer disc is characterized by a high ice content. We also showed that the combined effects of vertical settling and radial drift continuously change the chemical content of the disc.

Physical sorting and grain segregation are thought to be possible mechanisms that produced dust fractionation in pristine grains in the Solar nebula and the metal–silicate fractionation observed in meteorites (Kuebler et al. 1999; Zanda et al. 2006). This sorting may have been one of the mechanisms which produced the different chemical compositions among the different clans of chondrites and the differences found among chondrites groups belonging to the same clan (Palme & Jones 2003; Scott & Krot 2005; Wood 2005).

However, there is still a debate about the efficiency of aerodynamic sorting and on the location at which dust chemical sorting might have occurred. It has been suggested that different

evolutionary times and radial distances from the forming Sun had played a major role in determining the final structure of the chondrites parent bodies (Scott & Krot 2005).

In our simulation we are considering a large disc, thus we cannot directly compare our results with the chemical and dynamical evolution of the chondrites which formed in the inner Solar Nebula. However, an indirect comparison within the frame of our disc may help to find some analogies and determine if, when and where aggregates in our disc model can resemble the major properties of chondrites, and thus, suggest pathways of formation for these objects.

In the following discussion, we consider silicate and iron particles in our disc respectively as the possible chondrules precursors (or already formed chondrules) and the metallic grains in chondrites. The mechanism (or mechanisms) from which chondrules originated is still not well constrained [shock waves, planetesimals impacts, lightning, jets, winds (Scott & Krot 2005)], and more recent analysis suggests that chondrules formation may have started contemporaneously with CAIs (the oldest objects in our Solar system) in a continuous process which lasted ∼3 Myr (Connelly et al. 2012). As such it is not unreasonable to consider the presence of a sparse population of chondrules in the disc since the early stages of the protoplanetary disc evolution.

Our results show that radial chemical sorting characterizes the disc only when large scales are taken into consideration. The Fe/Si ratio in our inner mid-plane $20 < R\,(\mathrm{au}) < 100$ is always barely 'supersolar' with a deviation close to 1 per cent (see Fig. 11), while the Fe/Si of chondrites moves from solar (ordinary chondrites) towards sub-solar values (Righter et al. 2006) (see Fig. 2). Thus, aggregation of 'sub-solar' material in this location can be excluded.

We found that the Fe/Si in the mid-plane where $100 < R\,(\mathrm{au}) < 200$ (Fig. 12) is 'supersolar' until later stages ($t \sim 80$ kyr) when the fast radial drift starts to deplete the denser dust in this region. In this case assembling dust in this part of the mid-plane might lead to chemically fractionated aggregates, with 'sub-solar' Fe/Si ratios.

However, in order to produce fractionation in the outer mid-plane, time-scales of the order of 60 kyr are needed to lower the Fe/Si ratio from 1 to 0.9 (see Fig. 12). This is in case of a clean and efficient radial drift. Indeed, the radial drift of dust, and thus, the chemical sorting, can be slowed down and/or stopped by the presence of particle traps in the disc. Particles traps are thought to be locations at which a fast and efficient pile-up and growth of dust occurs, making the formation of larger planetesimals more favourable.

Particle traps can occur from the early stages of the protoplanetary disc evolution within vortices (Barge & Sommeria 1995; Johansen, Andersen & Brandenburg 2004), at the ice-lines and at the edge of the dead zone (Kretke & Lin 2007; Brauer, Henning & Dullemond 2008b), in discontinuities of the gas distribution in discs (Pinilla et al. 2012) or in self-induced dust traps (Gonzalez et al. 2015b, 2017). Particle traps can, thus, slow down or totally stop the radial chemical separation of the dust.

Vertical settling produces instead dust fractionation all along the disc surface (see Figs 11 and 12). The disc surface is the only region in which we find 'sub-solar' values of Fe/Si ratio from the beginning of our simulation. Aggregates in the surface of the disc can have 'solar' values of the Fe/Si ratio at the beginning of the simulation, and 'sub-solar' values a few thousands years later.

Furthermore, grain growth experienced by particles, and described in Section 3.1, suggests that aggregates with different Fe/Si ratios could also contain grains with different sizes. In Fig. 13 we superimpose, on the left column, the Fe/Si ratio and the average diameter of silicate and iron particles as a function of time, for the disc surface ($|Z\,(\mathrm{au})| > 1$) where $20 < R\,(\mathrm{au}) < 100$ (top), where $100 < R\,(\mathrm{au}) < 200$ (middle), and for the disc mid-plane ($-1 < Z\,(\mathrm{au}) < 1$) where $100 < R\,(\mathrm{au}) < 200$ (bottom). In the right column, we trace the ratio between the aerodynamic parameters of iron and silicate particles, $\zeta_{\mathrm{iron}}/\zeta_{\mathrm{sil}}$, as a function of time. The aerodynamic parameters are calculated using the average size of silicate and iron particles multiplied by their respective intrinsic densities. The closer the value of $\zeta_{\mathrm{iron}}/\zeta_{\mathrm{sil}}$ is to 1, the closer to a perfect size–density sorting the particles are. Thus, Fig. 13 allows to simultaneously check the chemical fractionation of the dust, the average grains diameter, and the aerodynamical sorting of grains in three different zones of the disc and at each time step of our simulation.

We see that aggregates with lower Fe/Si ratio will also have bigger grains. Furthermore, Fig. 13 (right column) shows that as soon as the simulation starts, the $\zeta_{\mathrm{iron}}/\zeta_{\mathrm{sil}}$ ratios move quickly towards values indicating a good degree of size–density sorting.

In the disc surface where $20 < R\,(\mathrm{au}) < 100$, values of Fe/Si < 1 are associated with grains diameter of the order of 0.1–1 mm and a $\zeta_{\mathrm{iron}}/\zeta_{\mathrm{sil}}$ value which can reach ∼1.2–1.1 over time-scales ranging between 8 and 18 kyr. In the disc surface where $100 < R\,(\mathrm{au}) < 200$, we see an Fe/Si < 1 ratio for the first 30 kyr, with grains having an average diameter of the order of 0.1–1 mm and with $\zeta_{\mathrm{iron}}/\zeta_{\mathrm{sil}}$ that can reach ∼1.1. At $t \sim 70$ kyr, the Fe/Si ratio drops a second time under 1, the grain diameter is of the order of mm and the $\zeta_{\mathrm{iron}}/\zeta_{\mathrm{sil}}$ ratio moves towards higher values. At this evolutionary stage, the total dust mass already dropped under 20 per cent of the initial amount (see Fig. 12), and thus, we are starting to sample the residual dust on the disc surface that did not grow/sort efficiently.

In the mid-plane where $100 < R\,(\mathrm{au}) < 200$, after $t \sim 80$ kyr, when the Fe/Si ratio moves to sub-solar values, the $\zeta_{\mathrm{iron}}/\zeta_{\mathrm{sil}}$ moves away from a perfect size–density sorting. However, the values of the $\zeta_{\mathrm{iron}}/\zeta_{\mathrm{sil}}$ ratios, when $80 < t(\mathrm{kyr}) < 140$, are still compatible with a good degree of aerodynamical sorting ($1 \leq \zeta_{\mathrm{iron}}/\zeta_{\mathrm{sil}} \leq 1.2$). Here, the average diameter of the iron and silicate particles when the Fe/Si starts to become 'sub-solar' is of the order of mm to cm (see Fig. 13 bottom). Aggregates in this region would have bigger grains (mm to cm), experience chemical fractionation and a general aerodynamical sorting. Then, as already shown in Fig. 10, at the end of the simulation, the residual aggregates in the outer discs will be less aerodynamically sorted although fractionation in their Fe/Si persists.

For completeness, we report in Fig. 14 the Fe/Si ratio, the average diameter of iron and silicate particles and the $\zeta_{\mathrm{iron}}/\zeta_{\mathrm{sil}}$ ratio for the inner mid-plane where $20 < R\,(\mathrm{au}) < 100$. It can be seen that particles in this zone of the disc move towards a perfect size–density sorting. The sorting in this zone is achieved almost immediately, just after the beginning of the simulation.

We thus find a trend that is compatible with a fractionation of the Fe/Si ratio and the size of the chondrules and iron grains found in different groups of chondrites. However, the values of the Fe/Si ratios returned by our simulations are not low enough when compared with the observed Fe/Si ratios in chondrites (Righter et al. 2006). This is because of our adopted spatial resolution. When calculating our ratios in the disc surface, we are considering, for a given interval in R, all the vertical extension of the disc for which ($|Z\,(\mathrm{au})| > 1$), thus losing resolution in Z.

Fig. 5 shows that there are zones in the disc surface for which the Fe/Si ratios can reach very low values, and 0 where iron particles are not present. Thus, as an example, we report in Fig. 15 the Fe/Si and the $\zeta_{\mathrm{iron}}/\zeta_{\mathrm{sil}}$ ratios for the disc surface where $|Z\,(\mathrm{au})| > 5$

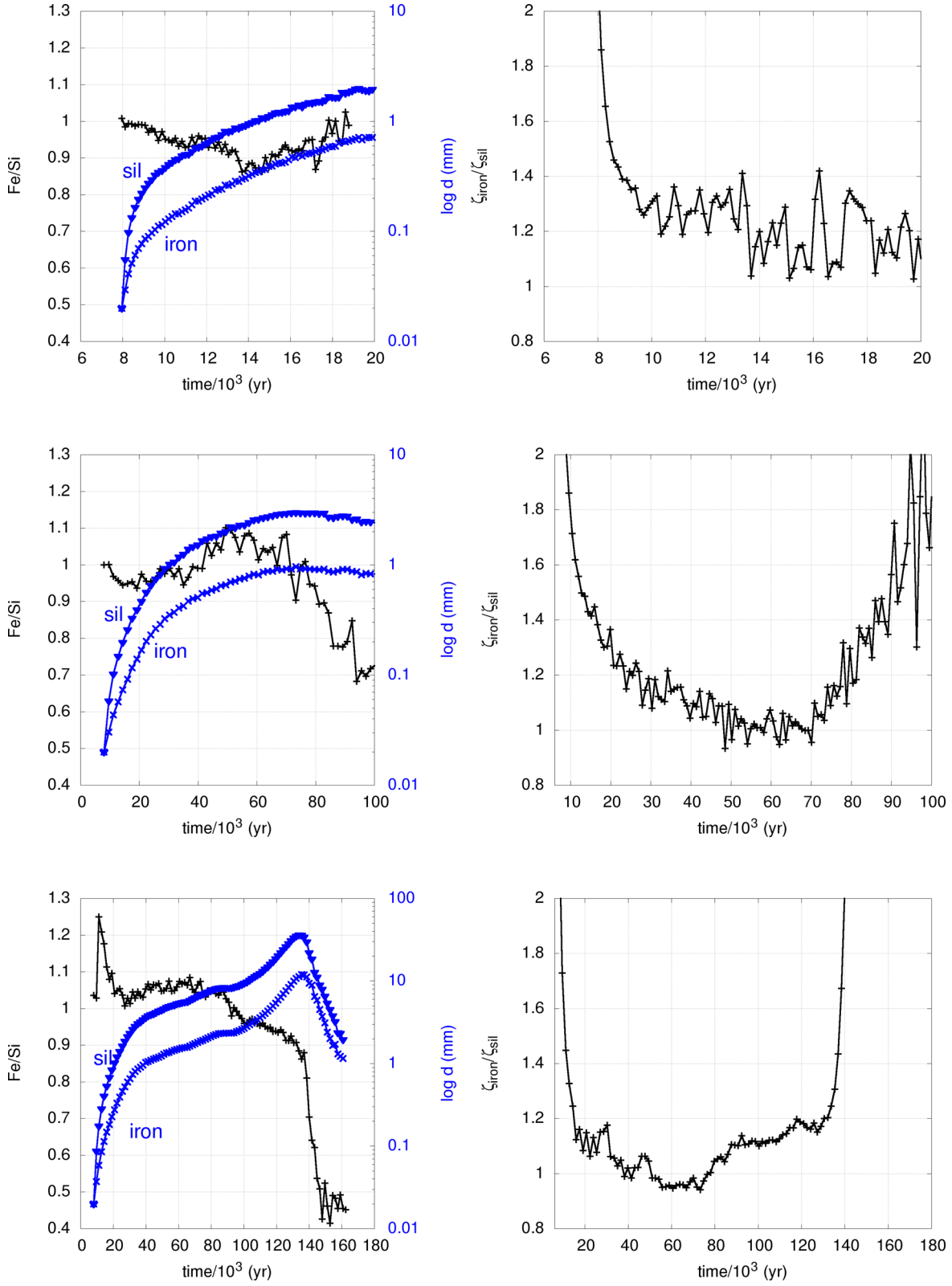

Figure 13. Left column: Fe/Si ratio (black) and average diameter of iron and silicate particles (blue) as a function of time. Top: disc surface ($|Z\,(\mathrm{au})| > 1$) where $20 < R\,(\mathrm{au}) < 100$. Middle: disc surface where $100 < R\,(\mathrm{au}) < 200$. Bottom: disc mid-plane ($-1 < Z\,(\mathrm{au}) < 1$) where $100 < R\,(\mathrm{au}) < 200$. Right column: $\zeta_{\mathrm{iron}}/\zeta_{\mathrm{sil}}$ for the three selected zones, calculated multiplying the average size of iron and silicates with their respective intrinsic densities. A perfect size–density sorting would occur when these ratios are equal to 1. The $\zeta_{\mathrm{iron}}/\zeta_{\mathrm{sil}}$ ratios decreases quickly towards 1 suggesting that the system evolves towards size–density sorting. However, in the outer surface, after 70 kyr, and in the mid-plane, after 80 kyr, when the Fe/Si ratio moves to 'sub-solar' values, the $\zeta_{\mathrm{iron}}/\zeta_{\mathrm{sil}}$ moves away from a perfect size–density sorting.

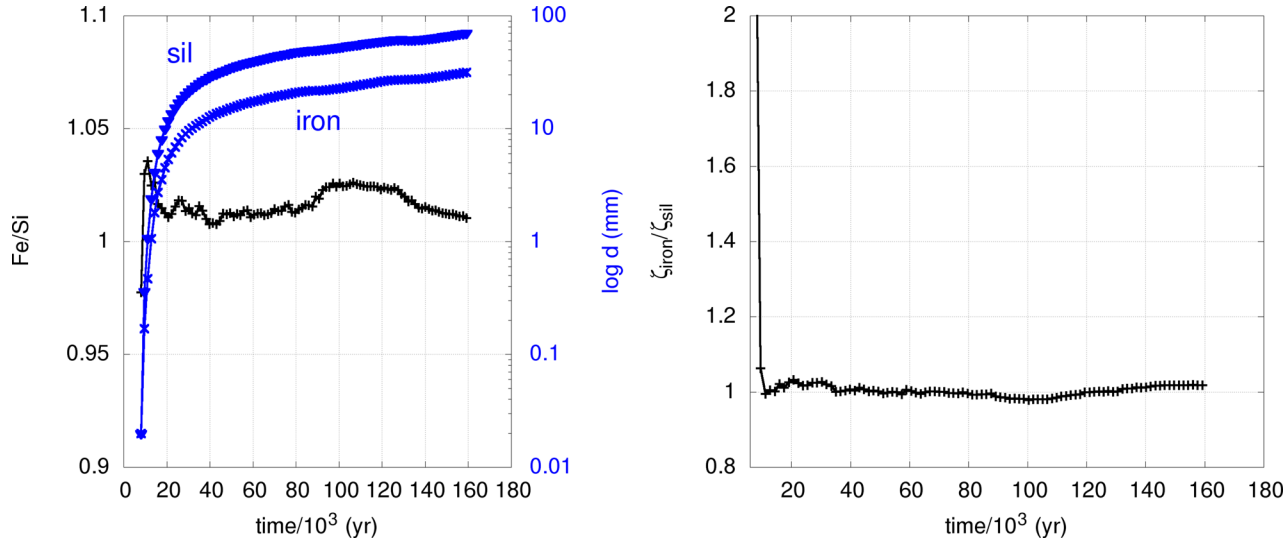

Figure 14. Left column: Fe/Si ratio (black) and average diameter of iron and silicate particles (blue) as a function of time for the disc mid-plane $[-1 < Z\,(\mathrm{au}) < 1]$ where $20 < R\,(\mathrm{au}) < 100$. Right column: $\zeta_{\mathrm{iron}}/\zeta_{\mathrm{sil}}$ for the selected zone, calculated multiplying the average size of iron and silicates with their respective intrinsic densities. A perfect size–density sorting would occur when these ratios are equal to 1. The $\zeta_{\mathrm{iron}}/\zeta_{\mathrm{sil}}$ ratio move quickly towards 1 suggesting that the in this zone of the disc, grains move toward a perfect sorting within few years after the beginning of the simulation.

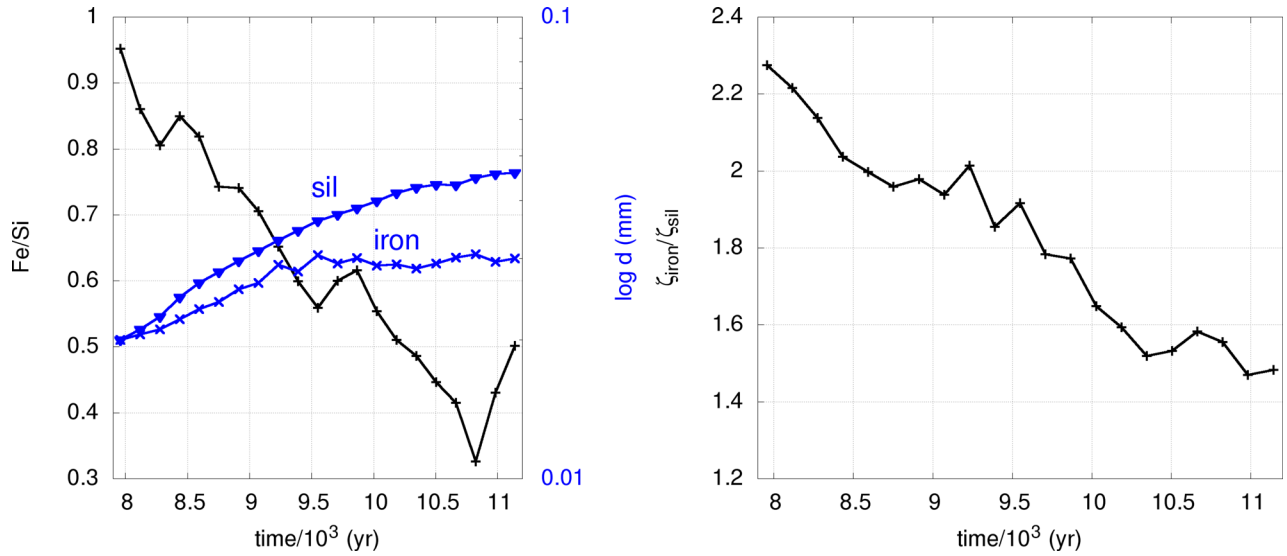

Figure 15. Left column: Fe/Si ratio (black) and average diameter of iron and silicate particles (blue) as a function of time for the disc surface ($|Z\,(\mathrm{au})| > 5$) where $20 < R\,(\mathrm{au}) < 100$. Right column: $\zeta_{\mathrm{iron}}/\zeta_{\mathrm{sil}}$ for the selected zone.

and $20 < R\,(\mathrm{au}) < 100$. Ratios are plotted until the number of iron particles reaches 0. It can be seen that, when a different vertical section of the disc is considered, the Fe/Si ratios can reach very low values, more compatible with the observed trend in chondrites, although, in this case, the size–density sorting is less efficient with a $\zeta_{\mathrm{iron}}/\zeta_{\mathrm{sil}}$ moving towards a minimum value of $\sim$1.4.

Furthermore, as already pointed out, chondrites did not form at this very large disc scales, but in the inner few au of our Solar nebula. This suggest that a similar process might have also occurred in the inner disc, with different time-scales or with different efficiency.

A simple extrapolation of our results would imply that the aggregation of chondritic material could have occurred in the surface of the inner young Solar Nebula during the two phases of vertical settling where size–density sorting was also efficient. The differences found among chondrites clans might then be ascribed to the different radial distance at which this process occurred. This distance could have then determined, for example, the amount of water accreted from the chondrite parent bodies. Indeed accretion of E chondrites likely occurred in the inner warmer region of the disc within the snow-line, ordinary chondrites close to the snow-line and carbonaceous chondrites beyond the snow-line (Scott & Krot 2005; Wood 2005).

These results only represent a starting point in the study of the dynamics of chondrites. Indeed, more complex models are needed to explain not only the variations in the Fe/Si ratios but also among other elements.

In our next study, we will explore the growth and the aerodynamic sorting of a multicomponent dust in the inner disc accounting also for dust fragmentation.

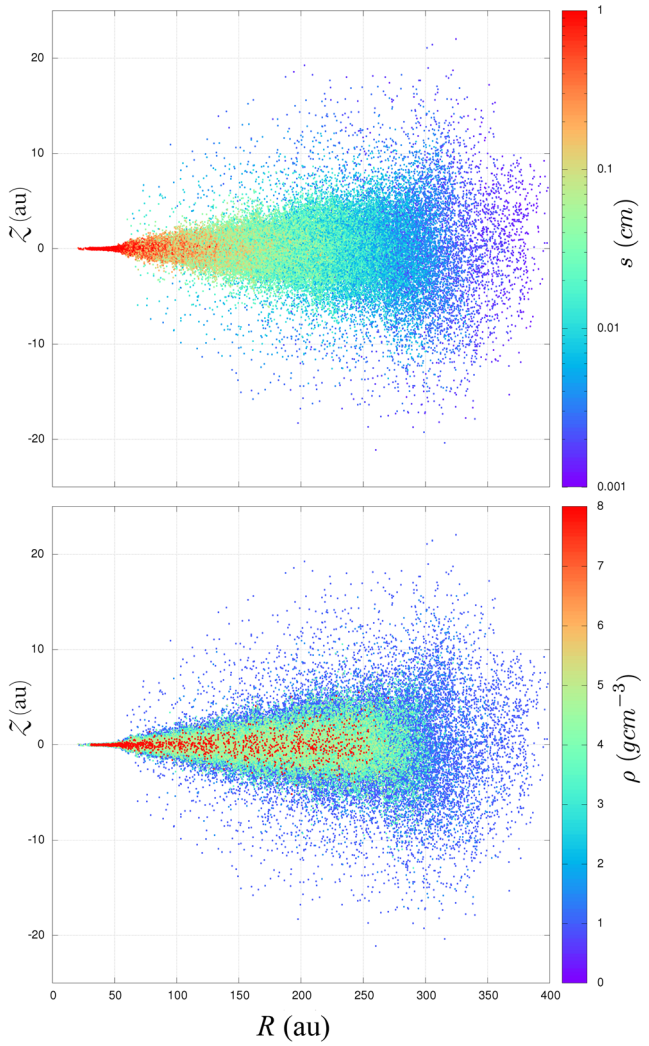

Figure 16. Top: grain size distribution as a function of R and Z at $t = 42\,970$ yr. Bottom: distribution of different chemical species as a function of R and Z. This figure reproduces the top-right panel in Fig. 5, for ease of comparison. Larger/heavier grains are located in the inner disc mid-plane while smaller/lighter grains are distributed in a wider zone. This in general agreement with observations.

4.3 Analogies with discs observations

In the previous sections, we showed that grains decouple from the gas and settle towards the mid-plane according to their density and size. Moreover, as grains reach their optimal drift size, they start to drift towards the inner region of the disc.

In Fig. 16 (top) we plot the grain size distribution at $t = 42\,970$ yr, as a function of R and Z. This time-step is the same as the top-right panel in Fig. 5 where we plotted ρ_d as a function of R and Z. That figure is reproduced in Fig. 16 (bottom) for ease of comparison.

In terms of size, our results are in good agreement with previous simulations made by Barrière-Fouchet et al. (2005) who studied the dust distribution of grains with different size and found that larger grains pile up in the disc mid-plane while smaller grains distribute in the disc envelope. We are also in agreement with the sorting trend observed in GG Tau and TW Hya described in Section 1.

Looking at the evolution of the chemical distribution in Fig. 5 and comparing it with the size distribution in Fig. 16, a qualitative observable prediction of the chemistry and physical properties of the dusty grains would read as smaller, lighter grains at the discs surface. This is in agreement with the dust properties of protoplanetary derived by infrared observation (Bouwman et al. 2008; Meeus et al. 2009) where micron-size silicates particles are used to fit the infra-red spectra of the surface of the dusty discs around young stellar objects.

Moreover, our results can help to disentangle the chemical dust composition of the disc within the mid-plane, which cannot be probed by observations (Williams & Cieza 2011). We suggest that the inner disc mid-plane could be enriched in denser material, iron and silicate-rich aggregates, while the outer disc regions would host ice-rich and iron-poor materials (see Fig. 8). This prediction is also consistent with the chemical radial gradient generally found in the Solar system when moving towards larger distances from the Sun (Lewis 2004): denser rocky planets in the inner regions while volatile-ice enriched bodies in the outer Solar system.

Furthermore, our results suggest that planetary embryos might accrete from inhomogeneous material since the beginning of their formation with the location (radius) of their accretion determining their initial bulk elemental ratios.

5 CONCLUSIONS

We presented SPH simulations of grain growth and sorting of multicomponent dust in a protoplanetary disc using a 3D, two-fluid (gas+dust) SPH code.

We found that the dust vertical settling is characterized by two phases: the first phase is driven by the dust density that leads to a vertical chemical sorting of the dust; the second phase is size-driven that allows the enhancement of the concentration of lighter material in the layers deep inside the disc. We also see an efficient radial chemical sorting of the dust, with denser material rapidly drifting in the inner zone of the disc. This process is driven by the different optimal drift size proper to each dust species.

Particles in the disc are aerodynamically (size and density) sorted in the inner regions, while in the outer regions the lower growth rates and the lower gas density prevent this sorting to occur efficiently. Particles move towards size–density sorting in very short timescales. Our results are compatible with the observed large scale dust sorting observed in protoplanetary discs.

We see that the growth and dynamics of a multicomponent dust clearly produce chemical fractionation and aerodynamic sorting in large disc scales. It is interesting to note that large discs ($20 \leq R$ (au) ≤ 400) could produce, in a very short time (for example, $t \sim 5$–20 kyr, in the inner disc surface), aggregates which would mimic the basic properties of chondrites. This suggests that dynamical chemical fractionation and aerodynamical sorting might have played an important role in determining their final aspect and chemical composition.

Moreover, our results open a new interesting question on the existence of undifferentiated and chemically fractionated aggregates which might have formed in the outer Solar Nebula during the early stages of the formation of our Solar system. We also suggest that planetary embryos might be characterized by inhomogeneous composition since the beginning of their formation.

ACKNOWLEDGEMENTS

The authors are grateful to the Lyon Institute of Origin (LIO) (ANR-10-LABX-0066) of the Université de Lyon for its financial support within the program 'Investissements d'Avenir' (ANR-11-IDEX-0007) of the French government operated by the National

Research Agency (ANR). We also acknowledge funding from PALSE (Programme Avenir Lyon Saint-Etienne). The authors wish to thank Sarah Maddison for helpful discussions and the anonymous referees for their useful comments that made us investigate in more detail our assumptions and the time-scales of dynamics and growth, which improved the manuscript. All simulations were performed at the Common Computing Facility of LABEX Lyon Institute of Origin (LIO).

REFERENCES

Amelin Y., Krot A. N., Hutcheon I. D., Ulyanov A. A., 2002, Science, 297, 1678
Andrews S. M. et al., 2012, ApJ, 744, 162
Bai X.-N., Stone J. M., 2010, ApJ, 722, 1437
Barge P., Sommeria J., 1995, A&A, 295, L1
Barrière-Fouchet L., Gonzalez J.-F., Murray J. R., Humble R. J., Maddison S. T., 2005, ApJ, 443, 185
Benoit P. H., Akridge G., Sears D. W. G., 1998, in Lunar Planet. Sci. Conf., Lunar and Planetary Institute, Houston, p. 1457
Birnstiel T., Dullemond C. P., Brauer F., 2010, A&A, 513, A79
Birnstiel T., Klahr H., Ercolano B., 2012, A&A, 539, A148
Blum J., Wurm G., 2000, Icarus, 143, 138
Blum J., Wurm G., 2008, ARA&A, 46, 21
Blum J. et al., 2000, Phys. Rev. Lett., 85, 2426
Bouwman J. et al., 2008, ApJ, 683, 479
Brauer F., Dullemond C. P., Henning T., 2008a, A&A, 480, 859
Brauer F., Henning T., Dullemond C. P., 2008b, A&A, 487, L1
Charnoz S., Taillifet E., 2012, ApJ, 753, 119
Ciesla F. J., 2007, ApJ, 654, L159
Ciesla F. J., 2009, Icarus, 200, 655
Clayton D. D., 1980, Earth Planet. Sci. Lett., 47, 199
Connelly J. N., Bizzarro M., Krot A. N., Nordlund Å., Wielandt D., Ivanova M. A., 2012, Science, 338, 651
Cuello N., Gonzalez J.-F., Pignatale F. C., 2016, MNRAS, 458, 2140
Cuzzi J. N., Weidenschilling S. J., 2006, in Lauretta D. S., McSween H. Y., eds, Meteorites and the Early Solar System II. Univ. Arizona Press, Tucson AZ, p. 353
Cuzzi J. N., Hogan R. C., Paque J. M., Dobrovolskis A. R., 2001, ApJ, 546, 496
Dominik C., Blum J., Cuzzi J. N., Wurm G., 2007, Protostars and Planets V. Univ. Arizona Press, Tucson AZ, p. 783
Drążkowska J., Alibert Y., Moore B., 2016, A&A, 594, A105
Dullemond C. P., Dominik C., 2004, ApJ, 421, 1075
Dullemond C. P., Dominik C., 2005, ApJ, 434, 971
Dullemond C. P., Dominik C., 2008, A&A, 487, 205
Fouchet L., Maddison S. T., Gonzalez J.-F., Murray J. R., 2007, ApJ, 474, 1037
Fouchet L., Gonzalez J.-F., Maddison S. T., 2010, A&A, 518, A16
Friedrich J. M., Weisberg M. K., Ebel D. S., Biltz A. E., Corbett B. M., Iotzov I. V., Khan W. S., Wolman M. D., 2015, Chemie der Erde/Geochemistry, 75, 419
Gail H.-P., 1998, ApJ, 332, 1099
Gonzalez J.-F., Laibe G., Maddison S. T., Pinte C., Ménard F., 2015a, P&SS, 116, 48
Gonzalez J.-F., Laibe G., Maddison S. T., Pinte C., Ménard F., 2015b, MNRAS, 454, L36
Gonzalez J.-F., Laibe G., Maddison S. T., 2017, MNRAS, 467, 1984
Haghighipour N., 2005, MNRAS, 362, 1015
Henning T., Semenov D., 2013, Chem. Rev., 113, 9016
Hughes A. M., Wilner D. J., Calvet N., D'Alessio P., Claussen M. J., Hogerheijde M. R., 2007, ApJ, 664, 536
Hughes A. M., Wilner D. J., Qi C., Hogerheijde M. R., 2008, ApJ, 678, 1119
Jacquet E., Gounelle M., Fromang S., 2012, Icarus, 220, 162
Johansen A., Andersen A. C., Brandenburg A., 2004, A&A, 417, 361
King A. R., Pringle J. E., Livio M., 2007, MNRAS, 376, 1740
Kretke K. A., Lin D. N. C., 2007, ApJ, 664, L55
Kuebler K. E., McSween H. Y., Carlson W. D., Hirsch D., 1999, Icarus, 141, 96
Laibe G., 2014, MNRAS, 437, 3037
Laibe G., Gonzalez J.-F., Fouchet L., Maddison S. T., 2008, A&A, 487, 265
Laibe G., Gonzalez J.-F., Maddison S. T., 2012, A&A, 537, A61
Laibe G., Gonzalez J.-F., Maddison S. T., 2014a, MNRAS, 437, 3025
Laibe G., Gonzalez J.-F., Maddison S. T., Crespe E., 2014b, MNRAS, 437, 3055
Larimer J. W., Anders E., 1970, Geochim. Cosmochim. Acta, 34, 367
Larimer J. W., Wasson J. T., 1988a, Meteorites and the Early Solar System. Univ. Arizona Press, Tucson, AZ, p. 394
Larimer J. W., Wasson J. T., 1988b, Meteorites and the Early Solar System. Univ. Arizona Press, Tucson, AZ, p. 416
Lewis J., 2004, Physics and Chemistry of the Solar system. Elsevier Academic Press, Burlington, MA
Liffman K., 2005, Meteorit. Planet. Sci., 40, 123
Lodato G., Rice W. K. M., 2004, MNRAS, 351, 630
MacPherson G. J., 2003, in Holland H. D., Turekian K. K., eds, Treatise on Geochemistry, Vol. 1. Pergamon Press, Oxford, p. 201
Martin R. G., Livio M., 2012, MNRAS, 425, L6
Meeus G. et al., 2009, A&A, 497, 379
Menu J. et al., 2014, A&A, 564, A93
Moore S. R., Franzen M., Benoit P. H., Sears D. W. G., Holley A., Meyer M., Godsey R., Czlapinski J., 2003, Geophys. Res. Lett., 30, 1522
Mumma M. J., Weissman P. R., Stern S. A., 1993, in Levy E. H., Lunine J. I., eds, Protostars and Planets III. Univ. Arizona Press, Tucson AZ, p. 1177
Okuzumi S., Tanaka H., Kobayashi H., Wada K., 2012, ApJ, 752, 106
Ormel C. W., Klahr H. H., 2010, A&A, 520, A43
Ormel C. W., Spaans M., Tielens A. G. G. M., 2007, A&A, 461, 215
Palme H., Jones A., 2003, in Turekian H. D. H. K., ed., Treatise on Geochemistry. Pergamon, Oxford, p. 41
Pinilla P., Birnstiel T., Ricci L., Dullemond C. P., Uribe A. L., Testi L., Natta A., 2012, A&A, 538, A114
Pinte C., Fouchet L., Ménard F., Gonzalez J.-F., Duchêne G., 2007, A&A, 469, 963
Pollack J. B., Hollenbach D., Beckwith S., Simonelli D. P., Roush T., Fong W., 1994, ApJ, 421, 615
Righter K., Drake M. J., Scott E. R. D., 2006, in Lauretta D. S., McSween H. Y., Jr, eds, Compositional Relationships Between Meteorites and Terrestrial Planets. Univ. Arizona Press, Tucson AZ, p. 803
Rubin A. E., 2010, Geochim. Cosmochim. Acta, 74, 4807
Sandford S. A., Allamandola L. J., 1993, Icarus, 106, 478
Scott E. R. D., 2007, Annu. Rev. Earth Planet. Sci., 35, 577
Scott E. R. D., Krot A. N., 2003, in Davis A. M., ed., Treatise on Geochemistry, Vol. 1. Elsevier, Oxford, p. 143
Scott E. R. D., Krot A. N., 2005, in Krot A. N., Scott E. R. D., Reipurth B., eds, ASP Conf. Ser. Vol. 341, Chondrites and the Protoplanetary Disk. Astron. Soc. Pac., San Francisco, p. 15
Shakura N. I., Sunyaev R. A., 1973, A&A, 24, 337
Stepinski T. F., Valageas P., 1997, A&A, 319, 1007
Suttner G., Yorke H. W., 2001, ApJ, 551, 461
Teiser J., Wurm G., 2009, MNRAS, 393, 1584
Testi L., Natta A., Shepherd D. S., Wilner D. J., 2003, A&A, 403, 323
Testi L. et al., 2014, Protostars and Planets VI. Univ. Arizona Press, Tucson, p. 339
Throop H. B., Bally J., Esposito L. W., McCaughrean M. J., 2001, Science, 292, 1686
Ubach C., Maddison S. T., Wright C. M., Wilner D. J., Lommen D. J. P., Koribalski B., 2012, MNRAS, 425, 3137
Wada K., Tanaka H., Suyama T., Kimura H., Yamamoto T., 2009, ApJ, 702, 1490
Wada K., Tanaka H., Okuzumi S., Kobayashi H., Suyama T., Kimura H., Yamamoto T., 2013, A&A, 559, A62
Weidenschilling S. J., 1977, MNRAS, 180, 57
Williams J. P., Cieza L. A., 2011, ARA&A, 49, 67
Wilner D. J., Ho P. T. P., Kastner J. H., Rodríguez L. F., 2000, ApJ, 534, L101

Wilner D. J., Bourke T. L., Wright C. M., Jørgensen J. K., van Dishoeck E. F., Wong T., 2003, ApJ, 596, 597
Wood J. A., 2005, in Krot A. N., Scott E. R. D., Reipurth B., eds, ASP Conf. Ser. Vol. 341, Chondrites and the Protoplanetary Disk. Astron. Soc. Pac., San Francisco, p. 953
Wurm G., Trieloff M., Rauer H., 2013, ApJ, 769, 78
Yamamoto T., Kadono T., Wada K., 2014, ApJ, 783, L36
Zanda B., Hewins R. H., Bourot-Denise M., Bland P. A., Albarède F., 2006, Earth Planet. Sci. Lett., 248, 650
Zsom A., Ormel C. W., Güttler C., Blum J., Dullemond C. P., 2010, A&A, 513, A57

APPENDIX A: DENSITY VERSUS GROWTH

In this appendix, we investigate the efficiency of grain growth, vertical settling and radial drift. Our aim is to confirm that growth is not efficient enough to erase the inhomogeneity that different grain densities bring in the disc since the beginning of our simulations.

If grains with initially comparable sizes and different densities are located at the same position, in order to counterbalance the dynamical differences driven by densities, lighter grains should reach the same aerodynamic parameter, ζ, as denser grains before the vertical settling and/or the radial drift separate them.

Using our disc model in its initial configuration, we first solve equation (5) with a simple numerical integration (see Laibe et al. 2008) for three different grains with the same $s_0 = 10\,\mu$m and different ρ_d (ice, silicates and iron, with ρ_d taken from Table 1). We assume that grains are located and locked in the same position. The chosen location is at $R = 100$ au, our reference radius, and $Z = H(R)$. We compute the time evolution of ζ and estimate the time, t_ζ, at which grains reach the same value of the aerodynamic parameter. The gas density at $Z = H(R)$ is calculated using

$$\rho_g(Z) = \frac{\Sigma}{\sqrt{2\pi}H} \exp\left(\frac{-Z}{2H}\right), \tag{A1}$$

in Laibe, Gonzalez & Maddison (2012). Then, we repeat the calculation in the mid-plane at $R = 100$ au. From Fig. 6 it can be seen that, once the particles reach the mid-plane, they have grown to sizes of the order of 100 μm. We thus use $s_0 = 100\,\mu$m as our reference size for this calculation.

Fig. A1 shows the time evolution of ζ for the three different particles calculated at $R = 100$ au at the disc surface $[Z = H(R)]$ for $s_0 = 10\,\mu$m (top) and in the mid-plane for $s_0 = 100\,\mu$m (bottom). Note the change of scales for ζ. The time-scales, t_ζ, for which three particles reach a similar value of ζ is of the order of $t_\zeta \sim 1000$ yr.

We now calculate the initial velocity of settling, v_{set}, and drift, v_{drift}, proper to each grain. These quantities, multiplied by an interval of time, t, give us an estimate of the separation which would occur between grains if they were allowed to move. We set $t = 1$ yr, a value much smaller than t_ζ. If the resulting separation between grains is not negligible we can conclude that growth cannot counterbalance the inhomogeneities that densities are bringing into the disc.

In our calculations, v_{set} is equal to

$$v_{set} = -\frac{\Omega_k^2 Z}{\rho_g c_s}\zeta, \tag{A2}$$

derived from equation (6), which is valid for small grain sizes (Dullemond & Dominik 2004).

v_{drift} is calculated using the following equation from Brauer et al. (2008a):

$$v_{drift} = v_{dust} + \frac{v_{gas}}{1 + (St^2)}. \tag{A3}$$

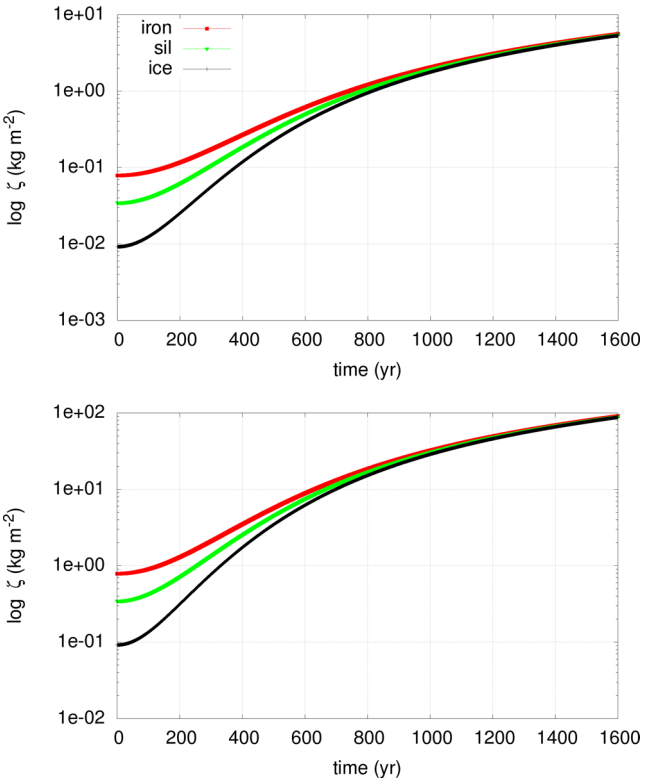

Figure A1. Time evolution of the aerodynamic parameter, ζ, at $R = 100$ au. Top, at the disc surface $[Z = H(R)]$ for $s_0 = 10\,\mu$m. Bottom, in the mid-plane for $s_0 = 100\,\mu$m.

Table A1. Radial separation at $R = 100$ au and $Z = 0$, between 100 μm size iron, silicate and ice particles (red) and vertical separation at $R = 100$ au and $Z = H(R)$, between 10 μm size iron, silicate and ice particles (black). Quantities are calculated after $t = 1$ yr and distances are expressed in km.

	Iron	Silicate	Ice
Iron	–	229	360
Silicate	16 790	–	132
Ice	26 460	9670	–

v_{dust} is given by

$$v_{dust} = -2\nu_n \frac{1}{St + (1/St)}, \tag{A4}$$

where

$$\nu = \frac{c_s^2}{2V}\left(\frac{7}{4} + p\right). \tag{A5}$$

v_{gas} is equal to

$$v_{gas} = -3\alpha\frac{c_s^2}{V}\left(\frac{3}{2} - p\right), \tag{A6}$$

where

$$V = \Omega R. \tag{A7}$$

In Table A1, we report the resulting radial, $\Delta R = (v^i_{drift} - v^j_{drift})t$, (red), and vertical, $\Delta Z = (v^i_{set} - v^j_{set})t$, (black), separation, in km, between particles with different densities, i, j, and the same initial

size, 10 μm, for the vertical settling from the disc surface, and 100 μm for the radial drift starting in the mid-plane.

Values in Table A1 show that drift and settling are very efficient processes which separate the particles well before they could reach the same ζ. Since all the calculated quantities scale according to the disc conditions, the separation of particles would occur at all disc radii, but with different time-scales.

These values are derived under the simple assumption that $v_{\rm drift}$ and $v_{\rm set}$ are constant in the considered small interval of time. Similarly, our estimation of t_ζ assumes that particles grow without moving. In reality $v_{\rm drift}$, $v_{\rm set}$ and $\mathrm{d}s/\mathrm{d}t$ change with time, local disc conditions and particles properties. Our code solves for all the quantities at play: in Figs 6 and 9 we showed the full pathways of settling, drift and growth, of particles that are located in the same position at the beginning of the simulation, and found that they separate quickly.

In conclusion, we see that growth is not efficient enough to counterbalance the different dynamical behaviour brought by densities since the early evolutionary stages. Dynamics will bring chemical heterogeneities in the disc where grains in different location will accrete from different available chemical reservoirs.

This paper has been typeset from a TEX/LATEX file prepared by the author.